

# Renormalisation group evolution effects on global SMEFT analyses

---

**Riccardo Bartocci, Anke Biekötter, Tobias Hurth**

*PRISMA+ Cluster of Excellence & Institute of Physics (THEP) & Mainz Institute for Theoretical Physics, Johannes Gutenberg University, D-55099 Mainz, Germany*

**ABSTRACT:** Global analyses in the Standard Model Effective Field Theory (SMEFT) framework serve as a tool to probe potential directions of new physics. To break degeneracies between the Wilson coefficients of the SMEFT, it is essential to combine observables from various experiments. Since different observables entering global fits may be measured at different energy scales, it becomes increasingly important to account for this fact through the renormalisation group evolution (RGE) of the Wilson coefficients. In this work, we investigate the effects of the RGE on a global SMEFT fit under the assumption of a  $U(3)^5$  symmetry within the minimal flavour violation framework. We comment on the role of next-to-leading order SMEFT predictions for breaking potential degeneracies between Wilson coefficients arising as a result of RGE effects.

---

## Contents

<b>1</b>	<b>Introduction</b>	<b>2</b>
<b>2</b>	<b>SMEFT assumptions and fit inputs</b>	<b>3</b>
2.1	Datasets	4
2.2	SMEFT predictions	4
<b>3</b>	<b>RGE effects</b>	<b>5</b>
<b>4</b>	<b>Single-parameter limits from RGE effects</b>	<b>6</b>
<b>5</b>	<b>Global analysis including RGE effects</b>	<b>7</b>
5.1	Partial next-to-leading order predictions	13
<b>6</b>	<b>Conclusions and outlook</b>	<b>13</b>
<b>A</b>	<b>Principal component analysis</b>	<b>15</b>
<b>B</b>	<b>Differences with respect to arXiv:2311.04963</b>	<b>16</b>
<b>C</b>	<b>Flavour symmetric and CP even operators</b>	<b>18</b>
<b>D</b>	<b>Observables</b>	<b>19</b>
<b>E</b>	<b>Numerical results</b>	<b>23</b>

---

# 1 Introduction

In the absence of direct new physics (NP) discoveries, Standard Model Effective Field Theory (SMEFT) [1–4] provides a powerful framework to describe deviations from the Standard Model (SM) expectation. Its main advantages lie in the minimal assumptions on the realisation of NP at a high and not currently experimentally accessible scale  $\Lambda$  and its systematic expansion in inverse powers of  $\Lambda$  and couplings.

Global SMEFT analyses play a crucial role in collecting experimental constraints on potential directions of new physics and assessing their status. They have been performed for various sectors of experimental observables including low-energy [5–7], flavour [8–11], electroweak [12–16] and top [17–21] data as well as combinations thereof [22–26]. To probe all directions of the NP parameter space in the SMEFT framework and break potential degeneracies between coefficients, it is crucial to combine observables from various experiments. For instance, electroweak precision observables (EWPO), Higgs and diboson data constrain different combinations of the Wilson coefficients contributing to the modification of  $Zq\bar{q}(h)$  couplings. As another example, degeneracies between semileptonic operators in Drell-Yan (DY) are broken in atomic parity violation and parity violation electron scattering [27].

Current global fits of LHC data are typically performed at the scale of the observables and assume that renormalisation group evolution (RGE) effects [28–30] between the various observables can be neglected. The inclusion of RGE effects between the scale of NP  $\Lambda$  and the scale of the observables, as needed for the interpretation in terms of NP models, is not generally given. However, the combination of observables measured at different scales within one global fit creates the need for the inclusion of RGE effects within the fit. While this is already standard in the analysis of flavour data, the relevance of RGE effects for high energy LHC and future collider SMEFT analyses has only recently received more attention [31–37], finding a sizeable impact of the running and mixing of the Wilson coefficients. Several studies have also highlighted the constraining power of present and future EWPO on four-quark operators and in particular those involving top quarks [38–41].

The aim of this paper is to assess the relevance of RGE effects on global SMEFT analyses including observables measured at a wide range of energy scales, from the sub-GeV level to kinematic distributions at several TeV. We perform an RGE improved global analysis of all CP even Wilson coefficients of the Warsaw basis [3] obeying a  $U(3)^5$  SMEFT symmetry at the high scale at tree level. This flavour assumption within the Minimal Flavour Violation (MFV) framework [42–45] reduces the number of independent Wilson coefficients to 41. It is motivated by the fact that flavour observables push the appearance of flavour-violating operators far above the TeV scale [46, 47]. The requirement of a  $U(3)^5$  symmetry for the SMEFT operators (at tree level) corresponds to a rather specific class of new physics models and reflects the minimal and unavoidable amount of flavour changing neutral currents (FCNCs) at the electroweak/low scale. Thereby, it can serve as a test case for a global analysis of an operator set motivated by a symmetry assumption with a manageable number of free coefficients. The lessons learned in this work are not expected to result in significantly different findings than a less restrictive flavour assumptions at the

high scale [48, 49].

We analyse the additional sensitivity gained on the Wilson coefficients provided by RGE effects on a single-parameter fit level, finding that EWPO, parity violation experiments (PVE) and DY provide additional constraints on four-quark operators. Moreover, we investigate RGE effects on a global SMEFT fit and discuss the origins of modifications to the limits of individual Wilson coefficients, focusing in particular on the cross talk of different observables and the new degeneracies appearing. We already anticipate that the largest effects are observed for the Wilson coefficients of four-quark operators and those that have strong correlations with them, in particular operators contributing to modified  $Zq\bar{q}(h)$  couplings.

The paper is organised as follows. In Section 2, we introduce the SMEFT framework and notations and give details on the observables and corresponding SMEFT predictions included in our fit. In Section 3, we give details on our treatment of RGE effects on the SMEFT predictions. In Sections 4 and 5, we present limits on the Wilson coefficients after the inclusion of RGE effects from a single-parameter fit and global fit, respectively. We conclude in Section 6. In Appendix A, we present a principal component analysis of our global fit. Appendix B is dedicated to a discussion of difference with respect to our previous work [25]. In Appendices C and D, we list the operators and observables included in our analysis. We present numerical results for the limits and correlation matrices in Appendix E.

## 2 SMEFT assumptions and fit inputs

The SMEFT Lagrangian, truncated at dimension six, is given by

$$\mathcal{L}_{\text{SMEFT}} = \mathcal{L}_{\text{SM}} + \sum_i \frac{C_i}{\Lambda^2} Q_i, \quad (2.1)$$

where  $C_i$  denote the Wilson coefficients of the operators  $Q_i$  in the Warsaw basis [3] and  $\Lambda$  denotes the NP scale, which we set to  $\Lambda = 4 \text{ TeV}$  throughout our work. We truncate all SMEFT predictions at linear order in the Wilson coefficients, neglecting quadratic contributions which are suppressed by  $\Lambda^{-4}$  and therefore formally of the same order as dimension-eight contributions. We employ the electromagnetic coupling constant, the mass of the  $Z$  boson and the Fermi constant  $\{\alpha, M_Z, G_F\}$  as our electroweak input parameters.

In order to reflect the minimal amount of FCNCs and CP violation observed at the electroweak scale, we make assumptions on the flavour structure of the NP interactions and their CP nature. We consider a  $U(3)^5$  symmetry of the SMEFT as initial condition at the high scale at tree level, specifically

$$U(3)^5 = U(3)_\ell \times U(3)_q \times U(3)_e \times U(3)_u \times U(3)_d, \quad (2.2)$$

where  $\{\ell, q, e, u, d\}$  represent the SM fermions [48]. This corresponds to the assumption that all new interactions of a model beyond the SM match onto flavour symmetric dimension-six operators at tree level. In addition, we restrict ourselves to CP-even interactions, as CP-odd ones can be much better constrained using dedicated search strategies [50–61]. These

two assumptions reduce the list of independent Wilson coefficients at dimension six to 41. We list the corresponding operators in Tab. 1. As already pointed out in the introduction, FCNCs at the electroweak scale are still predicted within our SMEFT flavour assumption, as a result of loop matching and RGE effects. However, all additional Wilson coefficients induced by these effects explicitly depend on the 41 parameters considered in our analysis.

## 2.1 Datasets

Our analysis combines observables measured at a wide range of energy scales, from the sub-GeV level to kinematic distributions at several TeV. Specifically, we include data from EWPO, diboson, Higgs, top, low-energy parity violation experiments (PVE), lepton scattering, flavour, DY as well as dijet+photon production. As this dataset almost exactly agrees with the one used for our previous study [25], we refer to this study for a detailed description of the included datasets and the Wilson coefficients constrained in each set and only comment on the differences with respect to [25] in this section. We also list the observables included in our fits in Appendix D, in Tables 2, 3, 4, and 5.

In addition to our previous dataset [25], we incorporate observables from  $\beta$ -decay and semileptonic meson decays as a single pseudo-observable,  $\Delta_{\text{CKM}}$ , which represents the unitarity of the CKM matrix [62–66]. We showed that this pseudo-observable mainly exhibits sensitivity to  $C_{lq}^{(3)}$  in a global fit [25]. Furthermore, we also include kinematic distributions of LHC diboson measurements from ATLAS in the  $WZ$  [67] and  $WW$  [68] final states. The impact of these additional datasets on the fit is discussed in Appendix B.

## 2.2 SMEFT predictions

We utilise SMEFT predictions from Ref. [69] (EWPO), `fitmaker` [22] (Higgs, top), Ref. [16] (Higgs), `SMEFiT` [23] ( $t\bar{t}$  at NLO), `flavio` [70] (flavour), Ref. [5, 71] (PVE, lepton scattering), `high-pT` [72] (Drell-Yan), Ref. [25] (dijet+photon production) and Ref. [66] ( $\Delta_{\text{CKM}}$ ). Some of these predictions assume flavour universality for the Wilson coefficients. To correctly account for the flavour dependence of the RGE effects, we reintroduce flavour coefficients in the predictions as follows. We assume that quark couplings to the Higgs boson as well as dipole operators are dominated by the third-generation quarks

$$C_{uG} \rightarrow C_{uG}_{33}, \quad C_{uW} \rightarrow C_{uW}_{33}, \quad C_{uB} \rightarrow C_{uB}_{33}, \quad C_{uH} \rightarrow C_{uH}_{33}, \quad C_{dH} \rightarrow C_{dH}_{33}, \quad (2.3)$$

where the notation  $C_{ij}^x$  is used for the flavour indices  $i$  and  $j$ . For top-sector predictions from `fitmaker`, third-generation indices are given explicitly and we assume that first- and second generation quarks equally contribute to the light-quark and lepton contributions, e.g.  $C_{Hl}^{(3)} \rightarrow 1/2(C_{Hl}^{(3)}_{11} + C_{Hl}^{(3)}_{22})$ .

For dijets+ $\gamma$  production, we regenerate the predictions including flavour indices using `SMEFTsim` [73]<sup>1</sup>. We give more details on this in Appendix B. The EWPO, DY, lepton scattering, PVE and flavour predictions are already flavour general, so no adjustments are needed.

---

<sup>1</sup>We attach these as an ancillary file to the arXiv submission.

With respect to [25], we have also fixed a bug in our translation of the Wilson coefficients from the basis of `SMEFTatNLO` [74] to the Warsaw basis.<sup>2</sup> This mistake changed the normalisation of the Wilson coefficients  $C_{qu}^{(x)}$ ,  $C_{qd}^{(x)}$  and  $C_{ud}^{(x)}$  with  $x = 1, 8$  in the top-sector SMEFT predictions by a factor of two and hence affected the top-dominated bounds by this factor. The discussion of the interplay of different datasets remains unchanged. We have also adjusted the sign of  $C_G$  such that all the Wilson coefficient definitions now agree with the ones employed in `SMEFTsim`.

### 3 RGE effects

The energy scale of the observables included in our fit ranges from below 1 GeV, as in the case of PVE, over the mass of the  $Z$  boson for EWPO, up to 2.3 TeV for kinematic distributions in DY and  $t\bar{t}$  production. To account for the scale dependence of the Wilson coefficients and facilitate the reinterpretation in terms of concrete models, we incorporate RGE effects into our SMEFT predictions. The importance of these effects for SMEFT analyses has been highlighted in [31–35].

In order to account for RGE effects, we need to assign a scale to each of our observables. As a baseline, we define the scale as the mass of the  $Z$  boson, the mass of the Higgs boson  $m_h$  and the mass of the top quark  $m_t$  in EWPO, Higgs and top-quark observables, respectively. In energy-dependent kinematic distributions, we use the invariant mass of the final state particles or the squared sum of a particle mass and its transverse momentum,  $\sqrt{m_i^2 + p_{T,i}^2}$ , as a scale measure. For bins in distributions, we use the lower edge of each bin as a measure of the scale of the process, as most distributions fall off quickly with enhanced energy. The scale assigned to each observable is explicitly listed in the last column of Tables 2, 3, 4, and 5 of Appendix D.

In the EFT framework, accounting for RGE effects is essential for the consistent perturbative treatment of quantum corrections at the low scale. To perform the RG evolution, we employ the `DsixTools` package [75–79]. Resummed leading-log RGE effects are included via its evolution matrix approach which allows us to express the evolution of the Wilson coefficients from a high scale  $\Lambda$  to a lower scale  $\mu$  as

$$C_i(\mu) = U_{ij}(\mu, \Lambda) C_j(\Lambda) \quad (3.1)$$

where  $U_{ij}$  denotes the evolution matrix. As already pointed out, we choose a fixed value of  $\Lambda = 4$  TeV throughout our study. This value is approximately twice the scale of the highest-energy observable included in our fit to ensure the validity of the EFT approach. Note that at scales  $\mu < \Lambda$ , the set of Wilson coefficients included in our analysis is no longer constrained to those obeying a  $U(3)^5$  symmetry as flavour non-conserving interactions are still allowed within the SM. However, all of the Wilson coefficients induced through the RGE are dependent on the 41 coefficients defined at the NP scale. Therefore, they do not correspond to independent NP directions in our fit and cannot induce any flat directions.

---

<sup>2</sup>We had not taken into account differences between the independent basis formulation of the Warsaw basis and its symmetric counterpart. Moreover, we copied an inconsistency in the relation between Wilson coefficients in the basis used by `SMEFTatNLO` and the Warsaw basis from [22].

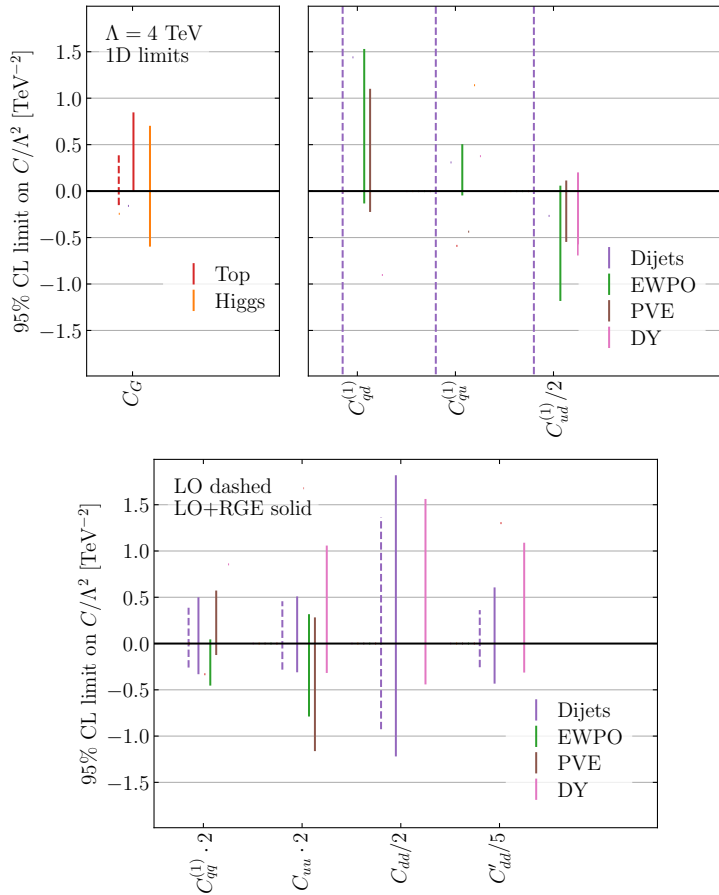


**Figure 1:** Single-parameter limits on the Wilson coefficients before (dashed) and after (solid) the inclusion of RGE effects from different datasets. We only display the strongest bound for the LO case and the LO+RGE bounds which are at most a factor two wider than the strongest bound in this setting. The different panels separate operators involving only gauge fields, four-quark operators with a suppressed interference in dijets+ $\gamma$  production and additional four-quark operators.

Taking into account RGE effects represents a crucial step forward in enhancing the precision of global analyses. In addition, the inclusion of RGE contributions serves as a probe to assess the importance of incorporating NLO effects in global fits. Although significant progress is being made on the automatization of the calculation of NLO predictions, automated results are currently only available for NLO QCD corrections [74]. Therefore, incorporating RGE effects in global SMEFT fits allows probing the relevance of NLO corrections consistently.

#### 4 Single-parameter limits from RGE effects

The inclusion of RGE mixing effects implies that operators defined at the high scale mix into operators defined at lower scales. Consequently, datasets that at LO do not constrain

certain coefficients can provide significant constraints through RGE effects. These newly introduced constraints can be competitive or even stronger than those present before RGE effects are included, in cases where LO constraints are weak.

We present in Fig. 1 the limits from single-parameter fits before (dashed lines) and after (solid lines) the inclusion of RGE effects for individual datasets. We show only the strongest bound for the LO case and the LO+RGE bounds that are at most a factor of two weaker than the strongest bound in this setting. For the coefficient  $C_G$ , the best constraints at LO and LO+RGE come from top quark processes. However, via mixing with the coefficient  $C_{HG}$ , the inclusion of RGE effects provides substantial additional constraints from Higgs data.

At LO, the only limits on the operators  $C_{qd}^{(1)}$ ,  $C_{qu}^{(1)}$ , and  $C_{ud}^{(1)}$  result from dijet+ $\gamma$  data. As the dijet production diagrams including the corresponding SMEFT operators and the dominant SM diagram do not interfere, the Wilson coefficients are poorly constrained at LO. When RGE effects are included, we observe additional limits from EWPO, PVE and DY on these coefficients. The mixing of  $C_{qd}^{(1)}$  and  $C_{ud}^{(1)}$  with the semileptonic operator  $C_{ed}$ , is responsible for the bounds from PVE and DY. Despite the fact that these mixing effects are suppressed by the electromagnetic coupling constant  $\alpha$ , they still lead to competitive constraints at the single-parameter fit level. This is a reflection of the fact that currently no dataset probes these coefficients well at LO. The constraints from EWPO result from the mixing of the considered four-quark operators with  $C_{Hu}$  and  $C_{Hd}$ , both of which are tightly constrained by EWPO.

The operator  $C_{qq}^{(1)}$  is dominantly constrained by dijet data at LO. This constraint remains relevant even when RGE effects are included, but after RGE, the most stringent bound comes from EWPO due to significant mixing with  $C_{Hq}^{(1)}$ . An additional constraint arises from PVE due to the mixing of  $C_{qq}^{(1)}$  and  $C_{qe}$ . The coefficient  $C_{uu}$  mixes with operator  $C_{Hu}$  and the semileptonic operators  $C_{eu}$  and  $C_{lu}$ , leading to additional bounds from EWPO, DY and PVE. Nevertheless, its dominant constraint still arises from dijet data. Finally, the operators  $C_{dd}$  and  $C'_{dd}$ , which at LO are constrained solely by dijet data, receive significant additional constraints from DY when mixing effects are included, even though the mixing of  $C_{dd}$  and  $C'_{dd}$  with semileptonic operators is suppressed by  $\alpha$ . For  $C_{dd}$ , DY even provides the strongest single-parameter constraint.

## 5 Global analysis including RGE effects

In this section, we present a global analysis based on RGE improved LO predictions. Following the procedure outlined in our previous analysis [25], we derive limits on a specific Wilson coefficient while profiling over the remaining parameters using the toy Monte Carlo method. We include correlations between different observables, where known.

In Figure 2, we show the 95% CL limits from a global fit on all 41 Wilson coefficients. We compare the bounds from the LO analysis (blue) and the RGE improved LO analysis (orange). We also show the limits from an RGE improved analysis based on partial NLO predictions (green), which we discuss in Section 5.1. Overall, we find that the inclusion of RGE effects helps remove the (almost) flat directions present in the LO fit. Specifically,



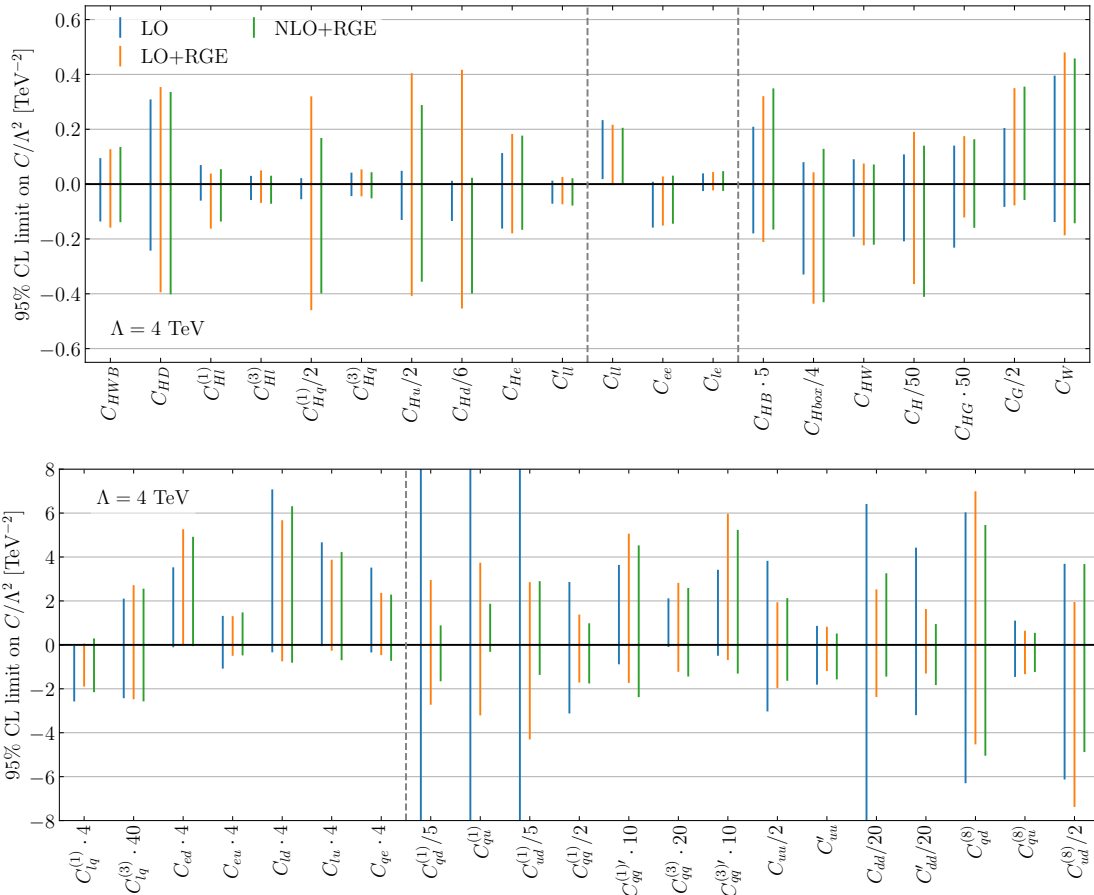


**Figure 2:** Comparison of the limits on the Wilson coefficients from a global fit purely based on LO predictions (LO), with those including RGE effects (LO+RGE) and including partial NLO predictions (NLO+RGE). Note that some Wilson coefficients have been scaled by appropriate factors on the  $x$  axis and that the  $y$  axis is different between the two panels.

it significantly improves the bounds on  $C_{qd}^{(1)}$ ,  $C_{qu}^{(1)}$ ,  $C_{ud}^{(1)}$  and  $C_{dd}$ , which are only weakly constrained at LO. To quantify this statement, we present the results of a principal component analysis (PCA) in Appendix A. In the following, we discuss the main differences between the LO fit and RGE improved LO fit for different Wilson coefficient categories.

**Operators contributing to EWPO at LO** The global limits on  $C_{Hq}^{(1)}$ ,  $C_{Hu}$  and  $C_{Hd}$ , which contribute to modified  $Zq\bar{q}(h)$  couplings, increase by factors 10.1, 4.5 and 5.9, respectively. This is the result of significant correlations between the quark-gauge operators and four-quark operators induced by the RG evolution. For  $C_{Hq}^{(3)}$ , which also contributes to modified  $Wq\bar{q}(h)$  interactions, correlations with four-quark operators are milder as a result of the additional constraints from  $W$  decay and  $Wh$  production. In the top left panel of Fig. 3, we show the correlations of  $C_{Hq}^{(1)}$ ,  $C_{Hu}$  and  $C_{Hd}$  with selected four-quark operators after including RGE effects in the fit. As one can see, several correlations are above the 50% level. To highlight how much of these correlations is due to the RGE

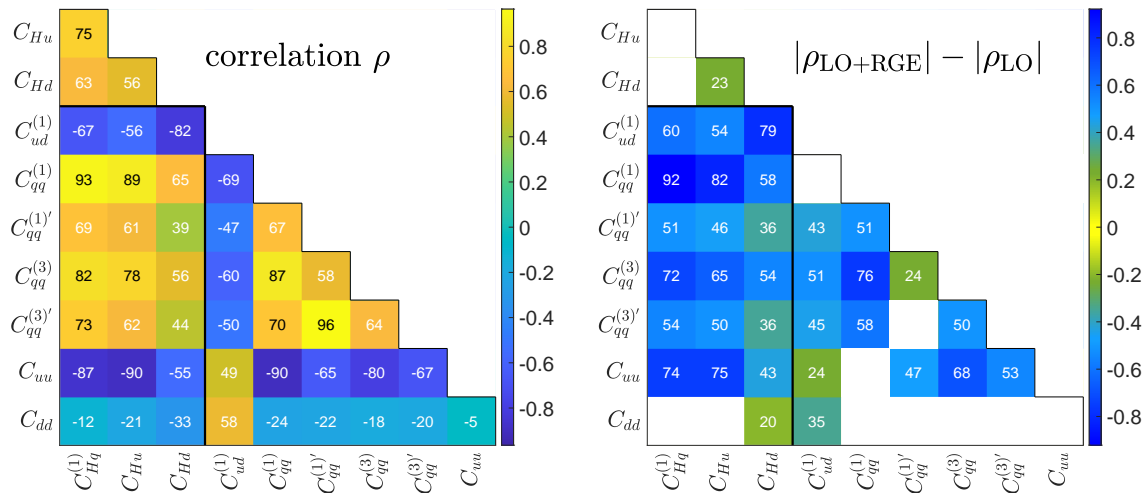


**Figure 3:** Left: Correlation  $\rho$  (in percent) between selected Wilson coefficients in the LO+RGE fit. Right: Difference between the absolute values of the correlations before and after the inclusion of RG evolution effects in the fit. Correlation changes below 20% have been omitted for better visibility of the dominant effects.

effects, in the top right panel of Fig. 3, we show the difference between the absolute values between before and after including RGE effects in the fit. The absolute correlations of the operators  $C_{Hq}^{(1)}$ ,  $C_{Hu}$ , and  $C_{Hd}$  with  $C_{ud}^{(1)}$ ,  $C_{qq}^{(1)}$ ,  $C_{qq}^{(1)'}$ ,  $C_{qq}^{(3)}$ ,  $C_{qq}^{(3)'}$ , and  $C_{uu}$  all increase by at least 36%. The strongest increases for each gauge-quark coefficient are an increase by 92% between  $C_{Hq}^{(1)}$  and  $C_{qq}^{(1)}$ , 82% between  $C_{Hu}$  and  $C_{qq}^{(1)}$ , and 79% between  $C_{Hd}$  and  $C_{ud}^{(1)}$ . Evidently, the RGE improvement induces strong correlations between the gauge-quark operators and several four-quark operators<sup>3</sup>. We have explicitly checked that removing four-quark operators from the fit would reduce the changes of the limits on  $C_{Hq}^{(1)}$ ,  $C_{Hu}$ , and  $C_{Hd}$  in an RGE improved LO fit to the 10% level. Even only removing the four-quark operators  $\{C_{uu}, C_{dd}, C_{dd}', C_{qq}^{(1)}, C_{qq}^{(3)}\}$ , which are often excluded or constrained to specific directions in top-centered global analyses, already reduces the effect of the RGE

<sup>3</sup>In our previous SMEFT fit based on partial NLO predictions [25], we noticed an increase of the limits on  $C_{Hq}^{(1)}$  by a factor two when including partial NLO EWPO predictions, while the limits on  $C_{Hu}$  and  $C_{Hd}$  only marginally changed. As the same diagrams contribute at NLO and in the RGE, this raises the question of why the correlation effects are stronger in the RGE improved fit than in the partial NLO fit. This is likely due to the fact that our NLO fit only includes partial NLO corrections. The lack of NLO predictions for  $Vh$  production leads to four-quark-operator-independent constraints on operators influencing quark-gauge interactions in the partial NLO fit. The oversimplification of the  $Zh$ -production prediction hence breaks degeneracies between the four-quark operators and  $C_{Hq}^{(1)}$ ,  $C_{Hu}$ ,  $C_{Hd}$ . For  $C_{Hq}^{(1)}$ , which has a reduced contribution to  $Zh$  production (compare to  $C_{Hu}$ ,  $C_{Hd}$  and  $C_{Hq}^{(3)}$ ) as a result of a cancellation between the contributions from up- and down-type quarks, this reduction of correlations with four-quark operators is less pronounced and we can already see its effect in the partial NLO fit. This highlights the relevance of further NLO SMEFT predictions, for instance for  $Zh$  production, which has recently been calculated for the production at lepton colliders [80].

improvement significantly, with limits still increasing by factors 2 – 3.

The Wilson coefficients of most other operators contributing to EWPO at LO are only mildly influenced by the RGE improvement. The bounds on  $C_{HD}$ ,  $C_{Hl}^{(1)}$  and  $C_{He}$  increase by 36%, 55% and 32%, respectively, as a result of increased correlations with various semileptonic operators. Diagonal running effects generally only play a subdominant role for the operators contributing to EWPO at LO. Accounting only for diagonal running effects, the bounds on  $C_{HD}$ ,  $C_{Hl}^{(1)}$  and  $C_{He}$  would only increase by 16%, 13% and 1%, respectively.

**Four-lepton operators** The four-lepton operators  $C_{ll}$ ,  $C_{ee}$ , and  $C_{le}$  are primarily constrained by lepton scattering processes at LO and exhibit minimal interplay with other datasets. Their RGE effects are suppressed by powers of  $\alpha$ . As expected, the limits on these coefficients remain largely unaffected by the inclusion of RGE effects, with global limits showing deviations of less than 7%. The bounds on  $C'_{ll}$ , which enters the SMEFT definition of the Higgs vacuum expectation value and thereby contributes to a larger set of observables, increases by 19% as a result of correlations.

**Higgs sector** The limits on most of the Wilson coefficients contributing mainly to Higgs physics do not significantly change after the inclusion of RGE effects. Increases and decreases of the limits in this sector are mostly dominated by diagonal running effects. For the coefficient  $C_{HG}$  the diagonal running contribution,  $C_{HG}(\Lambda) \approx 0.75 C_{HG}(m_H)$ <sup>4</sup>, dominates the decrease of the bound on this coefficient by around 20%. Similarly, the bound on  $C_H$  weakens by around 75% dominantly as a result of its diagonal running,  $C_H(\Lambda) \approx 1.45 C_H(m_H)$ .

We also note some shifts of the RGE improved fit limits with respect to the LO fit. As an example, we discuss here the shift of  $C_G$  towards more non-SM like values, which is strongly correlated with the shift of  $C_{HG}$ . The shift of  $C_G$  in the RGE improved fit is rooted in multiple ( $< 2\sigma$ ) deviations in Run I  $t\bar{t}$  production and the fact that it mixes with an operator with a different kinematic structure at the experimentally relevant scale.  $t\bar{t}$  production is sensitive to modifications of the top-gluon coupling as induced by  $C_{uG}$ <sub>33</sub>, which does not obey a  $U(3)$ <sup>5</sup> symmetry at the high scale  $\Lambda$ , but which receives sizable contributions from mixing with  $C_G$  at scales  $\mu < \Lambda$ .

CMS analysed Run I  $t\bar{t}$  data in a double differential distribution in the invariant mass  $m_{t\bar{t}}$  and rapidity  $y_{t\bar{t}}$  of the  $t\bar{t}$  system [81, 82]. In Fig. 4, we show the measured  $m_{t\bar{t}}$  distribution relative to the SM value. For each bin in  $m_{t\bar{t}}$ , we show the four measurements in the different rapidity bins. As one can see, all four measurements in the first  $m_{t\bar{t}}$  bin lie systematically above the SM prediction, while they lie systematically below the SM prediction in all remaining bins. In the same plot, we also show the SMEFT predictions when turning on a single Wilson coefficient  $C_G$  (blue solid line) or a single Wilson coefficient

<sup>4</sup>Note that we present  $C_i(\Lambda)$  as a function of its low scale definition  $C_i(\mu)$  here. The proportionality factor defined in this way corresponds more directly to the change of the limit between the LO fit, which sets constraints on  $C_i(\mu)$ , and the LO+RGE fit, which sets constraints on  $C_i(\Lambda)$ . If we presented  $C_i(\mu)$  as a function of  $C_i(\Lambda)$  instead, the limits would have an inverse proportionality.

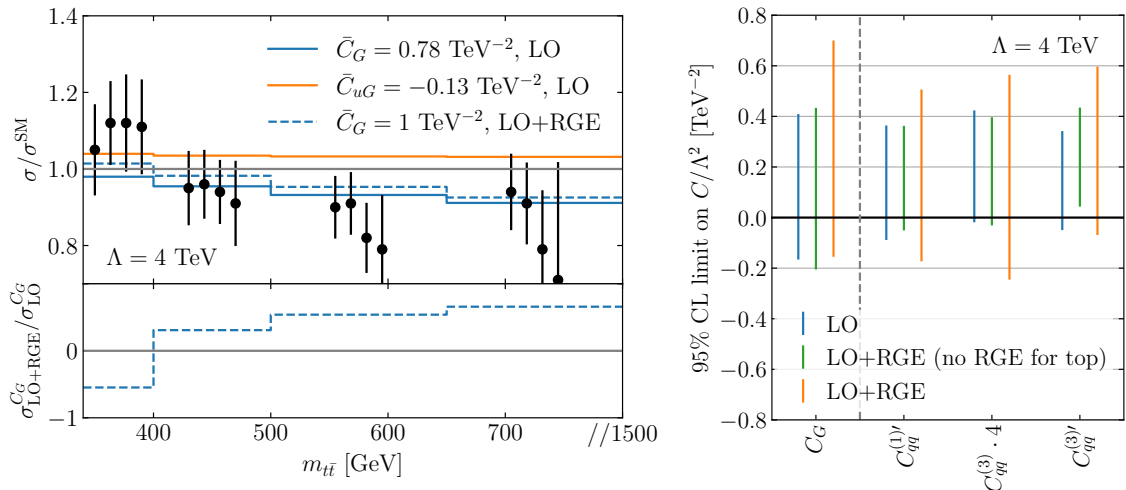


**Figure 4:** Left: SMEFT predictions for the  $m_{t\bar{t}}$  distribution in  $t\bar{t}$  production for the operators  $C_G$  and  $C_{uG}$ . We employ the notation  $\bar{C} = C/\Lambda^2$ . The reference values for  $\bar{C}_G$  and  $\bar{C}_{uG}$  refer to the RGE-induced contributions from  $\bar{C}_G(\Lambda) = 1 \text{ TeV}^{-1}$  at the scale  $\mu = 340 \text{ GeV}$ , see Eq. (5.1). The datapoints refer to the CMS Run I measurements in a double differential  $m_{t\bar{t}} - y_{t\bar{t}}$  distribution [81, 82]. Right: Limits on selected operators excluding RGE effects in SMEFT predictions for top-quark observables.

$C_{uG}$  (orange line) without including RGE effects. The values of the Wilson coefficients are chosen to match the RGE improved prediction from  $C_G(\Lambda) = 1$  at the scale of the first bin  $\mu = 340 \text{ GeV}$ ,

$$\begin{aligned} C_G(340 \text{ GeV}) &= 0.78 C_G(4 \text{ TeV}), \\ C_{uG}(340 \text{ GeV}) &= -0.13 C_G(4 \text{ TeV}). \end{aligned} \quad (5.1)$$

Moreover, we show the distribution for  $C_G$  when running down to  $m_{t\bar{t}}$  from  $\Lambda = 4 \text{ TeV}$  (dashed blue line). Due to a sign difference between the two contributions from  $C_G(\Lambda)$  in the SMEFT prediction, they partially cancel each other and lead to a sign flip of the  $C_G(\mu)$  prediction of the low- $m_{t\bar{t}}$  bin of the  $m_{t\bar{t}}$  kinematic distributions. As a result, positive values of  $C_G$  are able to improve the agreement with the data throughout all measurements when RG effects are included, thereby shifting the  $C_G$  limits towards positive values.

To further highlight that the shift of  $C_G$  is dominated by top sector data, we show in Fig. 4 (right) the limits from a global fit when excluding RGE effects in the top sector. As apparent from the plot, the limits on these two operators when excluding RGE effects in the top sector (green lines) match the limits from a fit excluding all RGE effects (blue lines) much more closely, and no shift is present.

Since both  $C_{uG}$  and  $C_G$  also enter the predictions of gluon-fusion Higgs production, they are correlated with  $C_{HG}$ . The shift of  $C_G$  in turn leads to a shift of  $C_{HG}$ .

**Semileptonic operators** Semileptonic operators exhibit notable mixing effects with four-quark operators. The most significant impact on the limits is observed for the op-

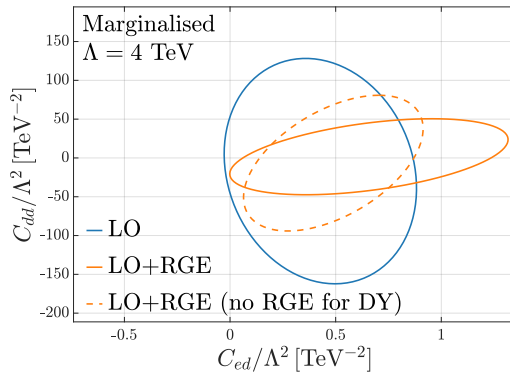


**Figure 5:** 95% CL limits on the Wilson coefficients  $C_{ed}$  and  $C_{dd}$  before and after the inclusion of RGE effects in a 2D plane.

erator  $C_{ed}$ , whose bound increases by 45%. In particular, the operators  $C_{dd}$  and  $C'_{dd}$ , which are among the least constrained in the global fit, mix into  $C_{ed}$ . Figure 5 illustrates the 95% CL contours for  $C_{ed}$  and  $C_{dd}$ , marginalising over the remaining 39 parameters. When RGE effects are included (orange continuous line), the constraint on  $C_{ed}$  is weakened compared to the LO fit without RGE (blue line). However, when the RGE contributions are removed from the DY dataset (orange dashed line) the bound on  $C_{ed}$  shrinks back to the blue contour, showing the impact of RGE effects in DY. Notably, the correlation between  $C_{ed}$  and  $C_{dd}$  increases from  $-15\%$  to  $45\%$  in the global fit after the inclusion of RGE effects.

Other semileptonic operators are less affected by RGE effects. The bounds on  $C_{eu}$ ,  $C_{lq}^{(1)}$  and  $C_{qe}$  decrease by 25% due to additional constraints from EWPO after the RGE improvement, which significantly reduces the correlation between selected semileptonic operators. For instance, the correlation between  $C_{lq}^{(1)}$  and  $C_{ed}$  reduces by 79%. Meanwhile, the bounds of the remaining coefficients change by less than 15%.

**Four-quark operators** The limits on individual four-quark operators significantly improve in the RG improved LO fit. As pointed out above, at LO, the Wilson coefficients  $C_{qd}^{(1)}$ ,  $C_{qu}^{(1)}$  and  $C_{ud}^{(1)}$  are only constrained by the dijets dataset. Since the corresponding operators do not interfere with the dominant SM diagram as a result of their colour structure, the bounds on these operators from an LO fit are weak, leaving (almost) blind directions in the fit. Through RGE effects, these operators are constrained in EWPO, PVE and DY, see also the single-parameter fit limits in Fig. 1. The mixing of  $C_{qd}^{(1)}$ ,  $C_{qu}^{(1)}$  and  $C_{ud}^{(1)}$  generates sizeable contributions to  $C_{Hu}$ ,  $C_{Hd}$  and  $C_{qu}^{(1)}$ . While the strong crosstalk of these and other four-quark coefficients leads to weaker bounds on the coefficients entering EWPO at LO, as discussed above, bounds on the four-quark coefficients in turn improve. For PVE and DY constraints, the dominant mixing effects are with the semileptonic operator  $C_{ed}$ . While limits from EWPO on  $C_{qd}^{(1)}$ ,  $C_{qu}^{(1)}$  and  $C_{ud}^{(1)}$  are stronger, they come with large correlations between these four-quark operators. PVE and DY allow to break these degeneracies.

Limits on  $C_{qq}^{(1)}$ ,  $C_{uu}$ ,  $C_{dd}$  and  $C'_{dd}$  improve by (40 – 70)%. As pointed out already in the discussion of single-parameter limits in Section 4, these coefficients receive additional constraints from DY, EWPO and PVE.

Limits on the coefficients  $C_{qq}^{(1)'}$ ,  $C_{qq}^{(3)}$ ,  $C_{qq}^{(3)'}$  weaken by (50 – 80)% in the RGE improved LO fit. RGE effects induce significant correlation increases between these four-quark operators, leading to broader bounds on the Wilson coefficients. These effects are dominated by RGE effects in the top sector, where these operators are tightly constrained, see right panel of Fig. 4. Neglecting RGE effects for the top-sector observables, the limits (green lines) on these three Wilson coefficients are in close agreement with those of the LO fit (blue lines).

The bounds on  $C'_{uu}$  as well as on the octet four-quark operators change by less than 25%.

### 5.1 Partial next-to-leading order predictions

Finite terms in next-to-leading order (NLO) SMEFT predictions tame some of the degeneracies in the global fit appearing as a result of the RGE improvement. As NLO SMEFT predictions are not known for all processes included in our fit, we only include partial NLO SMEFT predictions. Specifically, we include NLO predictions for EWPO [69, 83, 84],  $t\bar{t}h$  production [85], Higgs decays to gluons and photons  $h \rightarrow gg, \gamma\gamma$  [85],  $t\bar{t}$  production ( $m_{t\bar{t}}$  distribution and  $t\bar{t}$  charge asymmetries) [86, 87].

Formally, the inclusion of NLO SMEFT predictions requires the knowledge of two-loop RG equations. As these are currently only partially known [34, 88–93], we employ the one-loop RGE as a proxy.

In Fig. 2, we present the limits from our RGE improved partial NLO fit (green). Deviations from the RGE improved LO fit can be observed mainly for those operators which are directly impacted by the NLO SMEFT predictions. Correlations between  $C_{Hq}^{(1)}$ ,  $C_{Hu}$ ,  $C_{Hd}$  and four-quark operators are reduced by NLO SMEFT predictions for EWPO which results in stronger constraints on these Wilson coefficients. Limits on some four-quark operators contributing at NLO to  $t\bar{t}h$  ( $C_{qu}^{(1)}$ ) and  $t\bar{t}$  ( $C_{qd}^{(1)}$ ,  $C_{ud}^{(1)}$ ) production are also reduced when including NLO predictions for these datasets. The allowed ranges of all other Wilson coefficients are changed by at most 24% ( $C_{Hl}^{(3)}$ ).

## 6 Conclusions and outlook

The inclusion of RGE effects is a crucial advancement for the precision of global SMEFT analyses, allowing for the consistent combination of observables at different energy scales as well as their direct reinterpretation in terms of models defined at high scale. We present a global fit of the Wilson coefficients of the  $U(3)^5$  symmetric SMEFT to a dataset consisting of observables from EWPO, Higgs, top, flavour, PVE, DY and dijets+ $\gamma$  data and including RGE effects within the minimal flavour violation framework. We find that the limits on most coefficients are only mildly influenced by the inclusion of RGE effects. However, individual Wilson coefficients may also experience a significant decrease or increase of their

bounds as a result of correlations and crosstalk between observables induced through the RGE effects.

While the impact of the RGE improvement on some Wilson-coefficient bounds is dominated by diagonal running effects, e.g. for  $C_{HG}$ , the limits on others are mostly influenced by their mixing with other coefficients. The mixing introduces additional constraints on the coefficients from datasets to which they do not contribute at LO, as well as additional correlations between coefficients. A PCA has revealed a significant improvement of the four most weakly constrained directions in our global fit, which were poorly constrained at LO.

The Wilson coefficients corresponding to four-fermion operators are generally improved by the RGE effects, as they mix with operators well constrained in precision measurements. This is in particular true for the coefficients of operators with a suppressed interference with the SM at LO, specifically  $C_{qd}^{(1)}$ ,  $C_{qu}^{(1)}$  and  $C_{ud}^{(1)}$ . Moreover, the four-down-quark coefficients  $C_{dd}$  and  $C'_{dd}$ , which are only weakly constrained at LO, benefit from additional constraints resulting from their mixing with semileptonic operators.

On the other hand, limits on operators modifying the  $Zq\bar{q}(h)$  coupling,  $C_{Hq}^{(1)}$ ,  $C_{Hu}$ ,  $C_{Hd}$ , are significantly weakened in an RGE improved fit. This is the result of strong correlations between these coefficients and those corresponding to four-quark operators, which are generally much more weakly constrained. The modification of limits on operators contributing to EWPO at LO highlights the relevance of the inclusion of observables testing four-quark interactions in global SMEFT fits.

Finite terms in NLO SMEFT predictions may tame some of the degeneracies induced by RGE effects (as well as those present already at LO) and further improve the bounds in global fits. A conclusive remark on the effects of NLO SMEFT predictions will only be possible when more NLO predictions are available.

Overall, the inclusion of RGE effects in global SMEFT fits provides a more complete picture of the current status of experimental constraints and facilitates the interpretation in terms of specific models at the NP scale. Our study also highlights the interconnectedness of (flavour conserving) four-quark interactions with those tested in precision experiments. A generalisation to more generic flavour assumptions at the high scale within the MFV framework is left for future work.

## Acknowledgements

We thank Matthias König, Luca Mantani and Ken Mimasu for useful discussions. All three authors are supported by the Cluster of Excellence “Precision Physics, Fundamental Interactions, and Structure of Matter” (PRISMA<sup>+</sup> EXC 2118/1) funded by the German Research Foundation (DFG) within the German Excellence Strategy (Project ID 390831469). T.H. thanks the CERN theory group for its hospitality during his regular visits to CERN where part of the work was done.

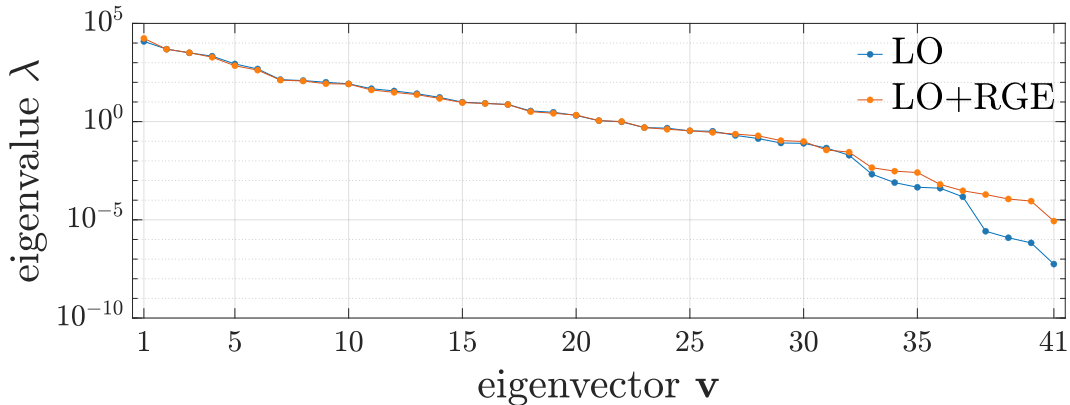


**Figure 6:** PCA analysis at LO (blue) and LO+RGE (orange). The eigenvalues of the Fisher matrix  $\lambda$  are shown for all the 41 eigenvectors  $\mathbf{v}$  in decreasing order.

## A Principal component analysis

In this appendix, we present the results of a principal component analysis (PCA) to examine how the least constrained directions are influenced by the RGE improvement. The Fisher information matrix,  $F(\theta)$ , is defined as:

$$F(\theta) = \frac{1}{2} \frac{\partial^2}{\partial C_i \partial C_j} \chi^2, \quad (\text{A.1})$$

where  $\chi^2$  is the chi squared function and  $C_i$  denote the Wilson coefficients. The eigenvalues  $\lambda_i$  of the Fisher matrix provide a measure of how good the directions spanned by the eigenvectors  $\mathbf{v}_i$  are constrained in the fit. If an eigenvector direction  $\mathbf{v}_i$  is unconstrained by the data, its corresponding Fisher matrix eigenvalue will be zero.

Figure 6 shows the eigenvalues of the Fisher matrix, associated with specific eigenvectors, plotted on a logarithmic scale and ordered from the most to the least constrained direction. The eigenvalues associated with the most constrained directions are very similar in the fits performed with and without RGE effects. However, the least constrained directions become significantly more constrained when RGE effects are included. In particular, we observe a notable reduction in the eigenvalues for the four least constrained directions. Among these, the least constrained direction differs by three orders of magnitude between the two fits, showing how the parameter space results more constrained when RGE is included.

As we point out in Section 5, the limits on individual Wilson coefficients can also be reduced in the RGE improved fit. This mostly concerns the operators  $C_{Hu}$ ,  $C_{Hd}$  and  $C_{Hq}^{(1)}$ . The increase of the bounds on these coefficients can also be seen in the PCA, where the coefficients  $C_{Hu}$  and  $C_{Hd}$  contribute to the seventh least constrained direction in the LO+RGE fit, corresponding to an eigenvalue  $\lambda_{35} = 2.6 \times 10^{-3}$ . In contrast, in the fit without RGE effects, these same coefficients first appear in a direction associated with an



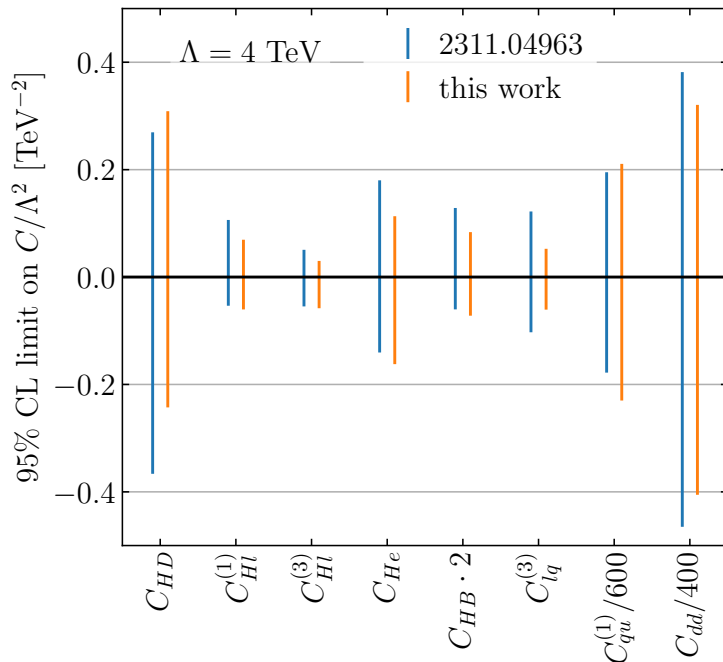


**Figure 7:** LO global analysis of all 41 Wilson coefficients using the dataset of Ref. [25] and using the dataset of the present paper. Only coefficients for which the bounds change by more than 15% on at least one side are shown.

eigenvalue  $\lambda_{24} = 4.7 \times 10^{-1}$ . This demonstrates that limits on these coefficients weaken when RGE effects are included.

## B Differences with respect to arXiv:2311.04963

In this appendix, we discuss the influence of differences in the datasets and predictions with respect to Ref. [25] on the global fit. We show in Figure 7 the comparison between the previous paper and the present work<sup>5</sup>, reporting those coefficients where the bounds changed on at least one side by more than 15%.

### Inclusion of $\Delta_{\text{CKM}}$ and diboson data

With respect to Ref. [25], we have added a pseudo-observable for  $\Delta_{\text{CKM}}$  as well as two kinematic distributions of  $WZ$  [67] and  $WW$  [68] production. Observables from  $\beta$ -decay and semileptonic meson decays [62, 63] have been shown to have an interesting interplay with EWPO [64–66]. As it was already done in the Appendix B of [25], we include these observables as a single pseudo-observable  $\Delta_{\text{CKM}}$  representing the unitarity of the CKM matrix. This inclusion has a sizeable impact on  $C_{lq}^{(3)}$  only.

Just like Higgs data, LHC diboson observables are known to break degeneracies present in EWPO. The inclusion of the diboson datasets reduces the allowed Wilson coefficient

<sup>5</sup>Factors of two in the normalisation of the Wilson coefficients of some four-quark operators, as discussed in Section 2.2 have been taken into account.

ranges of the operators contributing to EWPO at LO by up to 23%. The limits on the correlated Wilson coefficients  $C_{HB}$  improves at a similar level.

### EWPO predictions

In Ref. [25], we used EWPO SMEFT predictions from [83] which employs the on-shell definition  $\alpha^{\text{O.S.}}(0)$  as an input parameter. Here, we use the  $\overline{\text{MS}}$  definition of  $\alpha$  in a five-flavour version of QED $\times$ QCD as an input instead, and use the SMEFT predictions from [69]. This is more consistent with the input parameter choice for other observables included in our fit. Using a different renormalisation scheme for  $\alpha$  slightly modifies some prefactors of the EWPO SMEFT predictions. Using the updated EWPO SMEFT predictions in our global fit, we do not find effects above 15%.

### Dijets+ $\gamma$ predictions

In Ref. [25], we used predictions for ATLAS dijet plus photon production [94] determined with SMEFTsim [73] under the  $U(3)^5$ -model assumption. In this paper, due to the need of explicit flavour indices in order to correctly include RGE effects, we generated predictions under the general flavour assumption (model `SMEFTsim_general_alphaScheme_UFO`). We provide these new predictions as an ancillary file with the arXiv submission. We compare these new predictions, after restoring the flavour symmetry, with the previous ones and find an average deviation for each coefficient below 3%. In the global fit, this introduces some 15% deviations for the four-quark operators  $C_{qu}^{(1)}$  and  $C_{dd}$ .

## C Flavour symmetric and CP even operators

1 : $X^3$		2 : $H^6$		3 : $H^4 D^2$	
$Q_G$	$f^{ABC} G_\mu^{A\nu} G_\nu^{B\rho} G_\rho^{C\mu}$	$Q_H$	$(H^\dagger H)^3$	$Q_{H\Box}$	$(H^\dagger H)\Box(H^\dagger H)$
$Q_W$	$\epsilon^{IJK} W_\mu^{I\nu} W_\nu^{J\rho} W_\rho^{K\mu}$			$Q_{HD}$	$(H^\dagger D_\mu H)^* (H^\dagger D_\mu H)$
4 : $X^2 H^2$		7 : $\psi^2 H^2 D$			
$Q_{HG}$	$H^\dagger H G_{\mu\nu}^A G^{A\mu\nu}$	$Q_{Hl}^{(1)}$	$(H^\dagger i \overleftrightarrow{D}_\mu H)(\bar{l}_p \gamma^\mu l_p)$		
$Q_{HW}$	$H^\dagger H W_{\mu\nu}^I W^{I\mu\nu}$	$Q_{Hl}^{(3)}$	$(H^\dagger i \overleftrightarrow{D}_\mu^I H)(\bar{l}_p \tau^I \gamma^\mu l_p)$		
$Q_{HB}$	$H^\dagger H B_{\mu\nu} B^{\mu\nu}$	$Q_{He}$	$(H^\dagger i \overleftrightarrow{D}_\mu H)(\bar{e}_p \gamma^\mu e_p)$		
$Q_{HWB}$	$H^\dagger \tau^I H W_{\mu\nu}^I B^{\mu\nu}$	$Q_{Hq}^{(1)}$	$(H^\dagger i \overleftrightarrow{D}_\mu H)(\bar{q}_p \gamma^\mu q_p)$		
		$Q_{Hq}^{(3)}$	$(H^\dagger i \overleftrightarrow{D}_\mu^I H)(\bar{q}_p \tau^I \gamma^\mu q_p)$		
		$Q_{Hu}$	$(H^\dagger i \overleftrightarrow{D}_\mu H)(\bar{u}_p \gamma^\mu u_p)$		
		$Q_{Hd}$	$(H^\dagger i \overleftrightarrow{D}_\mu H)(\bar{d}_p \gamma^\mu d_p)$		
8 : $(\bar{L}L)(\bar{L}L)$		8 : $(\bar{R}R)(\bar{R}R)$		8 : $(\bar{L}L)(\bar{R}R)$	
$Q_{\ell\ell}$	$(\bar{l}_p \gamma_\mu l_p)(\bar{l}_s \gamma^\mu l_s)$	$Q_{ee}$	$(\bar{e}_p \gamma_\mu e_p)(\bar{e}_s \gamma^\mu e_s)$	$Q_{le}$	$(\bar{l}_p \gamma_\mu l_p)(\bar{e}_s \gamma^\mu e_s)$
$Q'_{\ell\ell}$	$(\bar{l}_p \gamma_\mu l_s)(\bar{l}_s \gamma^\mu l_p)$	$Q_{uu}$	$(\bar{u}_p \gamma_\mu u_p)(\bar{u}_s \gamma^\mu u_s)$	$Q_{lu}$	$(\bar{l}_p \gamma_\mu l_p)(\bar{u}_s \gamma^\mu u_s)$
$Q_{qq}^{(1)}$	$(\bar{q}_p \gamma_\mu q_p)(\bar{q}_s \gamma^\mu q_s)$	$Q'_{uu}$	$(\bar{u}_p \gamma_\mu u_s)(\bar{u}_s \gamma^\mu u_p)$	$Q_{ld}$	$(\bar{l}_p \gamma_\mu l_p)(\bar{d}_s \gamma^\mu d_s)$
$Q_{qq}^{(3)}$	$(\bar{q}_p \gamma_\mu \tau^I q_p)(\bar{q}_s \gamma^\mu \tau^I q_s)$	$Q_{dd}$	$(\bar{d}_p \gamma_\mu d_p)(\bar{d}_s \gamma^\mu d_s)$	$Q_{qe}$	$(\bar{q}_p \gamma_\mu q_p)(\bar{e}_s \gamma^\mu e_s)$
$Q_{qq}^{(1)'} $	$(\bar{q}_p \gamma_\mu q_s)(\bar{q}_s \gamma^\mu q_p)$	$Q'_{dd}$	$(\bar{d}_p \gamma_\mu d_s)(\bar{d}_s \gamma^\mu d_p)$	$Q_{qu}^{(1)}$	$(\bar{q}_p \gamma_\mu q_p)(\bar{u}_s \gamma^\mu u_s)$
$Q_{qq}^{(3)'} $	$(\bar{q}_p \gamma_\mu \tau^I q_s)(\bar{q}_s \gamma^\mu \tau^I q_p)$	$Q_{eu}$	$(\bar{e}_p \gamma_\mu e_p)(\bar{u}_s \gamma^\mu u_s)$	$Q_{qu}^{(8)}$	$(\bar{q}_p \gamma_\mu T^A q_p)(\bar{u}_s \gamma^\mu T^A u_s)$
$Q_{lq}^{(1)}$	$(\bar{l}_p \gamma_\mu l_p)(\bar{q}_s \gamma^\mu q_s)$	$Q_{ed}$	$(\bar{e}_p \gamma_\mu e_p)(\bar{d}_s \gamma^\mu d_s)$	$Q_{qd}^{(1)}$	$(\bar{q}_p \gamma_\mu q_p)(\bar{d}_s \gamma^\mu d_s)$
$Q_{lq}^{(3)}$	$(\bar{l}_p \gamma_\mu \tau^I l_p)(\bar{q}_s \gamma^\mu \tau^I q_s)$	$Q_{ud}^{(1)}$	$(\bar{u}_p \gamma_\mu u_p)(\bar{d}_s \gamma^\mu d_s)$	$Q_{qd}^{(8)}$	$(\bar{q}_p \gamma_\mu T^A q_p)(\bar{d}_s \gamma^\mu T^A d_s)$
		$Q_{ud}^{(8)}$	$(\bar{u}_p \gamma_\mu T^A u_p)(\bar{d}_s \gamma^\mu T^A d_s)$		

**Table 1:** Flavour symmetric and CP even dimension-six SMEFT operators in the Warsaw basis.

## D Observables

We list the observables included in our analysis in Tables 2-5. Table 2 lists observables from Higgs physics, LHC diboson and  $Zjj$  production, Tables 3 and 4 list observables from the top sector as well as Drell-Yan and dijet+photon data, and Table 5 lists observables from EWPO, PVE, lepton scattering and flavour.

**Table 2:** Higgs and electroweak observables included in the fit.

Observables		no. of measurements	scale(s)	References
<b>Higgs Data</b>		159		
7 and 8 TeV Run-I data	ATLAS & CMS combination	20	$M_H$	Table 8 of Ref. [95]
	ATLAS & CMS combination $\mu(h \rightarrow \mu\mu)$	1	$M_H$	Table 13 of Ref. [95]
	ATLAS $\mu(h \rightarrow Z\gamma)$	1	$M_H$	Figure 1 of Ref. [96]
13 TeV ATLAS Run-II data	$\mu(h \rightarrow Z\gamma)$ at 139 fb <sup>-1</sup>	1	$M_H$	[97]
	$\mu(h \rightarrow \mu\mu)$ at 139 fb <sup>-1</sup>	1	$M_H$	[98]
	$\mu(h \rightarrow \tau\tau)$ at 139 fb <sup>-1</sup>	4	$M_H$	Figure 14 of Ref. [99]
	$\mu(h \rightarrow bb)$ in VBF and $ttH$ at 139 fb <sup>-1</sup>	1+1	$M_H$	[100, 101]
	STXS $h \rightarrow \gamma\gamma/ZZ/b\bar{b}$ at 139 fb <sup>-1</sup>	42	$\sqrt{M_H^2 + (p_T^H)^2}$	Figures 1 and 2 of Ref. [102]
	STXS $h \rightarrow WW$ in ggF, VBF at 139 fb <sup>-1</sup>	11	$\sqrt{M_H^2 + (p_T^H)^2}$	Figures 12 and 14 of Ref. [103]
	di-Higgs $\mu_{HH}^{b\bar{b}b\bar{b}}, \mu_{HH}^{b\bar{b}\tau\bar{\tau}}, \mu_{HH}^{b\bar{b}\gamma\gamma}$	3	$M_H$	[104–106]
13 TeV CMS Run-II data	$\mu(h \rightarrow b\bar{b})$ in $Vh$ at 35.9/41.5 fb <sup>-1</sup>	2	$M_H$	Table 4 of Ref. [107]
	$\mu(h \rightarrow WW)$ in ggF at 137 fb <sup>-1</sup>	1	$M_H$	[108]
	$\mu(h \rightarrow \mu\mu)$ at 137 fb <sup>-1</sup>	4	$M_H$	Figure 11 of Ref. [109]
	$\mu(h \rightarrow \tau\tau/WW)$ in $t\bar{t}h$ at 137 fb <sup>-1</sup>	3	$M_H$	Figure 14 of Ref. [110]
	STXS $h \rightarrow WW$ at 137 fb <sup>-1</sup> in $Vh$	4	$\sqrt{M_H^2 + (p_T^H)^2}$	Table 9 of Ref. [111]
	STXS $h \rightarrow \tau\tau$ at 137 fb <sup>-1</sup>	11	$\sqrt{M_H^2 + (p_T^H)^2}$	Figures 11/12 of Ref. [112]
	STXS $h \rightarrow \gamma\gamma$ at 137 fb <sup>-1</sup>	27	$\sqrt{M_H^2 + (p_T^H)^2}$	Table 13 and Figure 21 of Ref. [113]
	STXS $h \rightarrow ZZ$ at 137 fb <sup>-1</sup>	18	$\sqrt{M_H^2 + (p_T^H)^2}$	Table 6 and Figure 15 of Ref. [114]
	di-Higgs $\mu_{HH}^{b\bar{b}b\bar{b}}, \mu_{HH}^{b\bar{b}\tau\bar{\tau}}, \mu_{HH}^{b\bar{b}\gamma\gamma}$	3	$M_H$	[115–117]
	ATLAS $Zjj$ 13 TeV $\Delta\phi_{jj}$ at 139 fb <sup>-1</sup>	12	$M_Z$	Figure 7(d) of Ref. [118]
ATLAS $WZ$ 13 TeV $p_T^Z$ at 36.1 fb <sup>-1</sup>	7	$\sqrt{M_Z^2 + (p_T^Z)^2}$	Figure 4(a) of Ref. [67]	
ATLAS $WW$ 13 TeV $p_T^{\ell, \text{lead}}$ at 36.1 fb <sup>-1</sup>	14	$\sqrt{M_W^2 + (p_T^{\ell, \text{lead}})^2}$	Figure 7(a) of Ref. [68]	

**Table 3:** Top physics observables from Tevatron and LHC Run I included in the fit.

Observables		no. of meas.	scale(s)	References
<b>Top Data from Tevatron and LHC Run I</b>		82		
Tevatron	forward-backward asymmetry $A_{FB}(m_{t\bar{t}})$ for $t\bar{t}$ production	4	$\max(m_t, m_{t\bar{t}})$	[119]
ATLAS & CMS	charge asymmetry $A_C(m_{t\bar{t}})$ for $t\bar{t}$ production in the $\ell$ +jets channel	6	$\max(m_t, m_{t\bar{t}})$	[120]
	$W$ -boson helicity fractions in top decay	3	$m_t$	[121]
ATLAS	charge asymmetry $A_C(m_{t\bar{t}})$ for $t\bar{t}$ production in the dilepton channel	1	$m_t$	[122]
	$\sigma_{t\bar{t}W}, \sigma_{t\bar{t}Z}$	2	$m_t$	[123]
	$\frac{d\sigma}{dp_T^T}, \frac{d\sigma}{d y_t^T }$ for $t$ -channel single-top production	4 + 5	$\sqrt{m_t^2 + (p_T^t)^2}, m_t$	[124]
	$\sigma_{tW}$ in the single lepton channel	1	$m_t$	[125]
	$\sigma_{tW}$ in the dilepton channel	1	$m_t$	[126]
	$s$ -channel single-top cross section	1	$m_t$	[127]
	$\frac{d\sigma}{dm_{t\bar{t}}}$ for $t\bar{t}$ production in the dilepton channel	6	$m_{t\bar{t}}$	[128]
	$\frac{d\sigma}{dp_T^T}$ for $t\bar{t}$ production in the $\ell$ +jets channel	8	$\sqrt{m_t^2 + (p_T^t)^2}$	[129]
CMS	$\sigma_{t\bar{t}\gamma}$ in the $\ell$ + jets channel	1	$m_t$	[130]
	charge asymmetry $A_C(m_{t\bar{t}})$ for $t\bar{t}$ production in the dilepton channel	3	$\max(m_t, m_{t\bar{t}})$	[131]
	$\sigma_{t\bar{t}W}, \sigma_{t\bar{t}Z}$	2	$m_t$	[130]
	$\sigma_{t\bar{t}\gamma}$ in the $\ell$ + jets channel.	1	$m_t$	[132]
	$s$ -channel single-top cross section	1	$m_t$	[133]
	$\frac{d\sigma}{dp_T^{t+\bar{t}}}$ of $t$ -channel single-top production	6	$\sqrt{m_t^2 + (p_T^t)^2}$	[134]
	$t$ -channel single-top and anti-top cross sections $R_t$	1	$m_t$	[135]
	$\sigma_{tW}$	1	$m_t$	[136]
	$\frac{d\sigma}{dm_{t\bar{t}}dy_{t\bar{t}}}$ for $t\bar{t}$ production in the dilepton channel	16	$m_{t\bar{t}}$	[81, 82]
	$\frac{d\sigma}{dp_T^T}$ for $t\bar{t}$ production in the $\ell$ +jets channel	8	$\sqrt{m_t^2 + (p_T^t)^2}$	[137, 138]

**Table 4:** Top physics observables from LHC Run II as well as data from Drell-Yan and dijet+photon production included in the analysis.

Observables		no. of meas.	scale(s)	References
<b>Top Data from LHC Run II</b>		55		
ATLAS	$\sigma_{tW}$	1	$m_t$	[139]
	$\sigma_{tZ}$	1	$m_t$	[140]
	$\sigma_{t+\bar{t}}, R_t$ for $t$ -channel single-top and anti-top cross sections	1+1	$m_t$	[141]
	charge asymmetry $A_C(m_{t\bar{t}})$ for $t\bar{t}$ production	5	$\max(m_t, m_{t\bar{t}})$	[142]
	$\sigma_{t\bar{t}W}, \sigma_{t\bar{t}Z}$	2	$m_t$	[143]
	$\frac{d\sigma}{dp_T^\gamma}$ for $t\bar{t}\gamma$ production	11	$\sqrt{m_t^2 + (p_T^\gamma)^2}$	[144]
CMS	$\sigma_{tW}$	1	$m_t$	[145]
	$\sigma_{tZ}$ in the $Z \rightarrow \ell^+ \ell^-$ channel	1	$m_t$	[146]
	$\frac{d\sigma}{dp_T^{t+\bar{t}}}$ and $R_t(p_T^{t+\bar{t}})$ for $t$ -channel single-top quark production	5 + 5	$\sqrt{m_t^2 + (p_T^t)^2}$	[147]
	$\frac{d\sigma}{dm_{t\bar{t}}}$ for $t\bar{t}$ production in the dilepton channel	6	$m_{t\bar{t}}$	[148]
	$\frac{d\sigma}{dm_{t\bar{t}}}$ for $t\bar{t}$ production in the $\ell$ +jets channel	15	$m_{t\bar{t}}$	[149]
	$\sigma_{t\bar{t}W}$	1	$m_t$	[150]
	$\frac{d\sigma}{dp_T^Z}$ for $t\bar{t}Z$ production	4	$\sqrt{m_t^2 + (p_T^Z)^2}$	[151]
<b>Drell-Yan</b>		109		
13 TeV	CMS $e^+e^-$ , $m_{ee}$	61 (up to 3 TeV)	$m_{ee}$	Figure 2 of [152]
	CMS $\mu^+\mu^-$ , $m_{\mu\mu}$	34 (up to 3 TeV)	$m_{\mu\mu}$	Figure 2 of [152]
	ATLAS $\tau^+\tau^-$ , $m_T^{\text{tot}}$	14 (up to 3 TeV)	$m_T^{\text{tot}}$	Figure 1 of [153]
<b>Dijets+photon</b>		26		
13 TeV	ATLAS $\frac{dN_{\text{cut}}}{dm_{jj}}$ for $pp \rightarrow jj\gamma + X$	26 (from 500 GeV)	$m_{jj}$	Figure 1 of [94]

**Table 5:** EWPO, PVE, lepton scattering and flavour observables included in the fit. For a summary of the experimental input values of the EWPO observables used, see also Tab. 3 of [83]. \* For scales below 5 GeV, we only include the LEFT RGE up to this scale. We explicitly checked that the evolution below 5 GeV is almost negligible when compared with the evolution between  $\Lambda$  and  $m_b$ .

Observables		no. of measurements	scale(s)	References
<b>Electroweak Precision Observables (EWPO)</b>		13	$M_Z$	[154]
<b>PVE and lepton scattering</b>		163		
PVE	$Q_W^{\text{Cs}}$	1	0.1 GeV*	[155]
	$Q_W^{\text{p}}$	1	0.1 GeV*	[156]
	$A_{1,2}^{\text{PVDIS}}$	2	1 GeV*	[157]
	SAMPLE	1	0.2 GeV*	[158]
lepton scattering	$\nu_\mu \nu_\mu ee$	2	0.1 GeV*	[155]
	$P_\tau, A_P$	2	58 GeV	[159]
	$g_{AV}^{ee}$ in $e^- e^- \rightarrow e^- e^-$	1	0.16 GeV*	[155]
	$A_{\text{FB}}^{\mu,\tau}$ in $e^+ e^- \rightarrow l^+ l^-$	24	$\sqrt{s}_{\text{LEP}}$	[160, 161]
	$\sigma_{\mu,\tau}$ in $e^+ e^- \rightarrow l^+ l^-$	24	$\sqrt{s}_{\text{LEP}}$	[160, 161]
	$\frac{d\sigma(ee)}{d\cos\theta}$ in $e^+ e^- \rightarrow l^+ l^-$	105	$\sqrt{s}_{\text{LEP}}$	[160, 161]
<b>Flavour</b>		37		
Differential BR( $B \rightarrow K\mu\mu$ ) (from 14 GeV)		3		[162]
Differential BR( $B \rightarrow K^*\mu\mu$ ) (from 14 GeV)		3	$m_b$	[163]
Differential BR( $\Lambda_b \rightarrow \Lambda\mu\mu$ ) (from 15 GeV)		1		[164]
BR( $B \rightarrow X_s\mu\mu, \mu\mu, X_s\gamma, K^*\gamma, K^{(*)}\bar{\nu}\nu$ )		5	$m_b$	[165–169]
BR( $B_s \rightarrow \mu\mu, \phi\gamma$ )		2	$m_b$	[166, 170]
BR( $K^+ \rightarrow \mu^+\nu_\mu$ )		1	$m_c^*$	[171]
$R_K$ and $R_K^*$		4	$m_b^*$	[172]
B meson mixing		2	$m_b$	[173]
K meson mixing		1	$m_c^*$	[174]
D meson mixing		8	$m_c^*$	[173]
Angular observables in $B \rightarrow K^*\mu\mu$ and $\Lambda_b \rightarrow \Lambda\mu\mu$ (from 15 GeV)		16	$m_b$	[164, 175]
$\Delta_{\text{CKM}}$		1	$M_Z$	[62, 63]

## E Numerical results

We present the correlation matrix of our global fit based on RGE improved LO SMEFT predictions in Figure 8. Numerical values for the results of the global fits based on LO, RGE improved LO and RGE improved NLO SMEFT predictions can be found in Table 6.

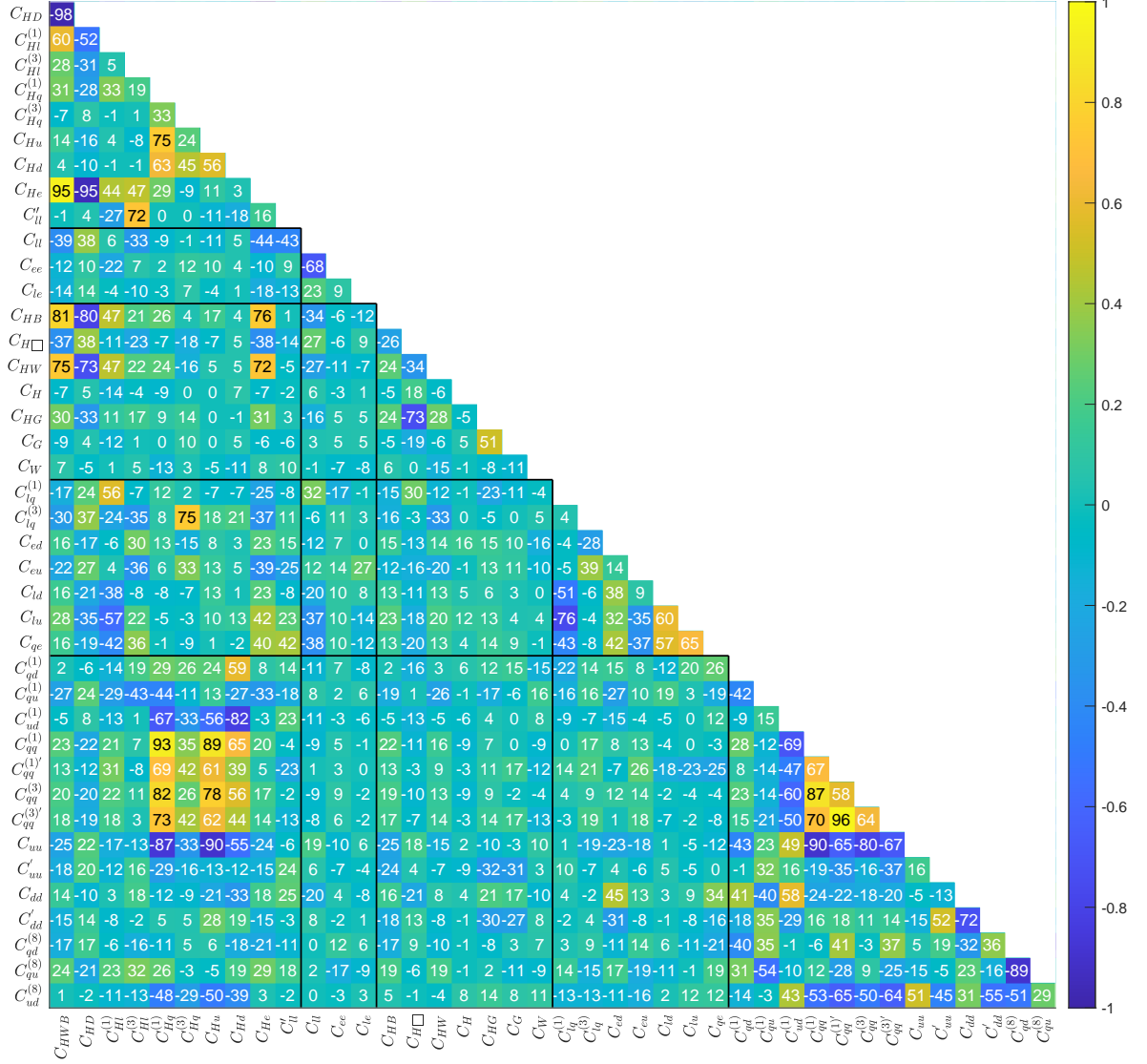


Figure 8: Correlation matrix of the LO global analysis including RGE effects. The numbers in the matrix correspond to the correlations in percent.



coefficient	global 95%CL limits		
	LO	LO+RGE	NLO+RGE
$C_{HWB}$	[-0.14, 0.09]	[-0.16, 0.13]	[-0.14, 0.14]
$C_{HD}$	[-0.24, 0.31]	[-0.39, 0.35]	[-0.4, 0.34]
$C_{Hl}^{(1)}$	[-0.06, 0.069]	[-0.16, 0.04]	[-0.14, 0.05]
$C_{Hl}^{(3)}$	[-0.058, 0.03]	[-0.069, 0.05]	[-0.072, 0.031]
$C_{Hq}^{(1)}$	[-0.11, 0.04]	[-0.92, 0.64]	[-0.8, 0.34]
$C_{Hq}^{(3)}$	[-0.044, 0.042]	[-0.045, 0.054]	[-0.052, 0.043]
$C_{Hu}$	[-0.26, 0.1]	[-0.82, 0.81]	[-0.71, 0.58]
$C_{Hd}$	[-0.81, 0.07]	[-2.7, 2.5]	[-2.4, 0.1]
$C_{He}$	[-0.16, 0.11]	[-0.18, 0.18]	[-0.17, 0.18]
$C'_{ll}$	[-0.072, 0.013]	[-0.074, 0.026]	[-0.078, 0.021]
$C_{ll}$	[0.02, 0.23]	[-0.0, 0.22]	[0.0, 0.21]
$C_{ee}$	[-0.16, 0.01]	[-0.15, 0.03]	[-0.14, 0.03]
$C_{le}$	[-0.025, 0.039]	[-0.023, 0.044]	[-0.025, 0.047]
$C_{HB}$	[-0.036, 0.042]	[-0.042, 0.064]	[-0.033, 0.07]
$C_{H\Box}$	[-1.3, 0.3]	[-1.7, 0.2]	[-1.7, 0.5]
$C_{HW}$	[-0.19, 0.09]	[-0.22, 0.08]	[-0.22, 0.07]
$C_H$	[-10, 5]	[-18, 9]	[-20, 7]
$C_{HG}$	[-0.005, 0.003]	[-0.002, 0.003]	[-0.003, 0.003]
$C_G$	[-0.17, 0.41]	[-0.16, 0.7]	[-0.12, 0.71]
$C_W$	[-0.14, 0.4]	[-0.19, 0.48]	[-0.14, 0.46]
$C_{lq}^{(1)}$	[-0.64, -0.01]	[-0.47, 0.02]	[-0.54, 0.07]
$C_{lq}^{(3)}$	[-0.061, 0.053]	[-0.062, 0.068]	[-0.064, 0.064]
$C_{ed}$	[-0.03, 0.88]	[-0.0, 1.3]	[-0.0, 1.2]
$C_{eu}$	[-0.27, 0.33]	[-0.12, 0.33]	[-0.12, 0.37]
$C_{ld}$	[-0.1, 1.8]	[-0.2, 1.4]	[-0.2, 1.6]
$C_{lu}$	[-0.0, 1.2]	[-0.07, 0.97]	[-0.2, 1.1]
$C_{qe}$	[-0.09, 0.88]	[-0.12, 0.59]	[-0.18, 0.57]
$C_{qd}^{(1)}$	[-730, 670]	[-13, 14]	[-8.3, 4.4]
$C_{qu}^{(1)}$	[-140, 130]	[-3.2, 3.7]	[-0.3, 1.9]
$C_{ud}^{(1)}$	[-170, 220]	[-21, 14]	[-6, 14]
$C_{qq}^{(1)}$	[-6.2, 5.7]	[-3.4, 2.8]	[-3.5, 2.0]
$C_{qq}^{(1)'} $	[-0.09, 0.36]	[-0.17, 0.51]	[-0.24, 0.45]
$C_{qq}^{(3)}$	[-0.0, 0.11]	[-0.06, 0.14]	[-0.07, 0.13]
$C_{qq}^{(3)'} $	[-0.05, 0.34]	[-0.07, 0.6]	[-0.13, 0.52]
$C_{uu}$	[-6.1, 7.7]	[-3.9, 3.9]	[-3.3, 4.3]
$C'_{uu}$	[-1.8, 0.9]	[-1.2, 0.8]	[-1.6, 0.5]
$C_{dd}$	[-160, 130]	[-47, 50]	[-28, 65]
$C'_{dd}$	[-63, 88]	[-26, 32]	[-36, 18]
$C_{qd}^{(8)}$	[-6.3, 6.0]	[-4.5, 7.0]	[-5.0, 5.5]
$C_{qu}^{(8)}$	[-1.5, 1.1]	[-1.3, 0.6]	[-1.2, 0.5]
$C_{ud}^{(8)}$	[-12, 7]	[-14, 3]	[-9.8, 7.4]

**Table 6:** Numerical results of the global analyses based on LO, RGE improved LO and RGE improved NLO SMEFT predictions.

## References

- [1] W. Buchmuller and D. Wyler, *Effective Lagrangian Analysis of New Interactions and Flavor Conservation*, *Nucl. Phys. B* **268** (1986) 621–653.
- [2] F. Wilczek, *Problem of Strong P and T Invariance in the Presence of Instantons*, *Phys. Rev. Lett.* **40** (1978) 279–282.
- [3] B. Grzadkowski, M. Iskrzynski, M. Misiak and J. Rosiek, *Dimension-Six Terms in the Standard Model Lagrangian*, *JHEP* **10** (2010) 085, [[1008.4884](#)].
- [4] I. Brivio and M. Trott, *The Standard Model as an Effective Field Theory*, *Phys. Rept.* **793** (2019) 1–98, [[1706.08945](#)].
- [5] A. Falkowski, M. González-Alonso and K. Mimouni, *Compilation of low-energy constraints on 4-fermion operators in the SMEFT*, *JHEP* **08** (2017) 123, [[1706.03783](#)].
- [6] A. Falkowski, M. González-Alonso and Z. Tabrizi, *Reactor neutrino oscillations as constraints on Effective Field Theory*, *JHEP* **05** (2019) 173, [[1901.04553](#)].
- [7] A. Falkowski, M. González-Alonso, O. Naviliat-Cuncic and N. Severijns, *Superallowed decays within and beyond the standard model*, *Eur. Phys. J. A* **59** (2023) 113.
- [8] R. Aoude, T. Hurth, S. Renner and W. Shepherd, *The impact of flavour data on global fits of the MFV SMEFT*, *JHEP* **12** (2020) 113, [[2003.05432](#)].
- [9] S. Bruggisser, R. Schäfer, D. van Dyk and S. Westhoff, *The Flavor of UV Physics*, *JHEP* **05** (2021) 257, [[2101.07273](#)].
- [10] S. Bruggisser, D. van Dyk and S. Westhoff, *Resolving the flavor structure in the MFV-SMEFT*, *JHEP* **02** (2023) 225, [[2212.02532](#)].
- [11] C. Grunwald, G. Hiller, K. Kröninger and L. Nollen, *More synergies from beauty, top, Z and Drell-Yan measurements in SMEFT*, *JHEP* **11** (2023) 110, [[2304.12837](#)].
- [12] A. Biekötter, T. Corbett and T. Plehn, *The Gauge-Higgs Legacy of the LHC Run II*, *SciPost Phys.* **6** (2019) 064, [[1812.07587](#)].
- [13] S. Kraml, T. Q. Loc, D. T. Nhung and L. D. Ninh, *Constraining new physics from Higgs measurements with Lilith: update to LHC Run 2 results*, *SciPost Phys.* **7** (2019) 052, [[1908.03952](#)].
- [14] S. Dawson, S. Homiller and S. D. Lane, *Putting standard model EFT fits to work*, *Phys. Rev. D* **102** (2020) 055012, [[2007.01296](#)].
- [15] E. d. S. Almeida, A. Alves, O. J. P. Éboli and M. C. Gonzalez-Garcia, *Electroweak legacy of the LHC run II*, *Phys. Rev. D* **105** (2022) 013006, [[2108.04828](#)].
- [16] Anisha, S. Das Bakshi, S. Banerjee, A. Biekötter, J. Chakraborty, S. Kumar Patra et al., *Effective limits on single scalar extensions in the light of recent LHC data*, *Phys. Rev. D* **107** (2023) 055028, [[2111.05876](#)].
- [17] A. Buckley, C. Englert, J. Ferrando, D. J. Miller, L. Moore, M. Russell et al., *Constraining top quark effective theory in the LHC Run II era*, *JHEP* **04** (2016) 015, [[1512.03360](#)].
- [18] D. Barducci et al., *Interpreting top-quark LHC measurements in the standard-model effective field theory*, [1802.07237](#).

- [19] I. Brivio, S. Bruggisser, F. Maltoni, R. Moutafis, T. Plehn, E. Vryonidou et al., *O new physics, where art thou? A global search in the top sector*, *JHEP* **02** (2020) 131, [[1910.03606](#)].
- [20] S. Bißmann, J. Erdmann, C. Grunwald, G. Hiller and K. Kröninger, *Constraining top-quark couplings combining top-quark and  $B$  decay observables*, *Eur. Phys. J. C* **80** (2020) 136, [[1909.13632](#)].
- [21] G. Durieux, A. Irlles, V. Miralles, A. Peñuelas, R. Pöschl, M. Perelló et al., *The electro-weak couplings of the top and bottom quarks — Global fit and future prospects*, *JHEP* **12** (2019) 98, [[1907.10619](#)].
- [22] J. Ellis, M. Madigan, K. Mimasu, V. Sanz and T. You, *Top, Higgs, Diboson and Electroweak Fit to the Standard Model Effective Field Theory*, *JHEP* **04** (2021) 279, [[2012.02779](#)].
- [23] SMEFT collaboration, J. J. Ethier, G. Magni, F. Maltoni, L. Mantani, E. R. Nocera, J. Rojo et al., *Combined SMEFT interpretation of Higgs, diboson, and top quark data from the LHC*, *JHEP* **11** (2021) 089, [[2105.00006](#)].
- [24] F. Garosi, D. Marzocca, A. R. Sánchez and A. Stanzione, *Indirect constraints on top quark operators from a global SMEFT analysis*, *JHEP* **12** (2023) 129, [[2310.00047](#)].
- [25] R. Bartocci, A. Biekötter and T. Hurth, *A global analysis of the SMEFT under the minimal MFV assumption*, *JHEP* **05** (2024) 074, [[2311.04963](#)].
- [26] E. Celada, T. Giani, J. ter Hoeve, L. Mantani, J. Rojo, A. N. Rossia et al., *Mapping the SMEFT at high-energy colliders: from LEP and the (HL-)LHC to the FCC-ee*, *JHEP* **09** (2024) 091, [[2404.12809](#)].
- [27] R. Boughezal, F. Petriello and D. Wiegand, *Disentangling Standard Model EFT operators with future low-energy parity-violating electron scattering experiments*, *Phys. Rev. D* **104** (2021) 016005, [[2104.03979](#)].
- [28] E. E. Jenkins, A. V. Manohar and M. Trott, *Renormalization Group Evolution of the Standard Model Dimension Six Operators I: Formalism and lambda Dependence*, *JHEP* **10** (2013) 087, [[1308.2627](#)].
- [29] E. E. Jenkins, A. V. Manohar and M. Trott, *Renormalization Group Evolution of the Standard Model Dimension Six Operators II: Yukawa Dependence*, *JHEP* **01** (2014) 035, [[1310.4838](#)].
- [30] R. Alonso, E. E. Jenkins, A. V. Manohar and M. Trott, *Renormalization Group Evolution of the Standard Model Dimension Six Operators III: Gauge Coupling Dependence and Phenomenology*, *JHEP* **04** (2014) 159, [[1312.2014](#)].
- [31] M. Battaglia, M. Grazzini, M. Spira and M. Wiesemann, *Sensitivity to BSM effects in the Higgs  $p_T$  spectrum within SMEFT*, *JHEP* **11** (2021) 173, [[2109.02987](#)].
- [32] R. Aoude, F. Maltoni, O. Mattelaer, C. Severi and E. Vryonidou, *Renormalisation group effects on SMEFT interpretations of LHC data*, *JHEP* **09** (2023) 191, [[2212.05067](#)].
- [33] S. Di Noi and R. Gröber, *Renormalisation group running effects in  $pp \rightarrow t\bar{t}h$  in the Standard Model Effective Field Theory*, *Eur. Phys. J. C* **84** (2024) 403, [[2312.11327](#)].
- [34] S. Di Noi, R. Gröber and M. K. Mandal, *Two-loop running effects in Higgs physics in Standard Model Effective Field Theory*, [2408.03252](#).

- [35] G. Heinrich and J. Lang, *Renormalisation group effects in SMEFT for di-Higgs production*, [2409.19578](#).
- [36] F. Maltoni, G. Ventura and E. Vryonidou, *Impact of SMEFT renormalisation group running on Higgs production at the LHC*, [2406.06670](#).
- [37] K. Asteriadis, S. Dawson, P. P. Giardino and R. Szafron, *Prospects for New Discoveries Through Precision Measurements at  $e^+e^-$  Colliders*, [2406.03557](#).
- [38] A. Greljo, A. Palavrić and A. Smolkovič, *Leading directions in the SMEFT: Renormalization effects*, *Phys. Rev. D* **109** (2024) 075033, [[2312.09179](#)].
- [39] L. Allwicher, C. Cornella, G. Isidori and B. A. Stefanek, *New physics in the third generation. A comprehensive SMEFT analysis and future prospects*, *JHEP* **03** (2024) 049, [[2311.00020](#)].
- [40] U. Haisch and L. Schnell, *Precision tests of third-generation four-quark operators: matching SMEFT to LEFT*, [2410.13304](#).
- [41] J. Gargalionis, J. Quevillon, P. N. H. Vuong and T. You, *Linear Standard Model extensions in the SMEFT at one loop and Tera-Z*, [2412.01759](#).
- [42] J. M. Gerard, *FERMION MASS SPECTRUM IN  $SU(2)_L \times U(1)$* , *Z. Phys. C* **18** (1983) 145.
- [43] R. S. Chivukula and H. Georgi, *Composite Technicolor Standard Model*, *Phys. Lett. B* **188** (1987) 99–104.
- [44] L. J. Hall and L. Randall, *Weak scale effective supersymmetry*, *Phys. Rev. Lett.* **65** (1990) 2939–2942.
- [45] G. D’Ambrosio, G. F. Giudice, G. Isidori and A. Strumia, *Minimal flavor violation: An Effective field theory approach*, *Nucl. Phys. B* **645** (2002) 155–187, [[hep-ph/0207036](#)].
- [46] L. Calibbi and G. Signorelli, *Charged Lepton Flavour Violation: An Experimental and Theoretical Introduction*, *Riv. Nuovo Cim.* **41** (2018) 71–174, [[1709.00294](#)].
- [47] L. Silvestrini and M. Valli, *Model-independent Bounds on the Standard Model Effective Theory from Flavour Physics*, *Phys. Lett. B* **799** (2019) 135062, [[1812.10913](#)].
- [48] D. A. Faroughy, G. Isidori, F. Wilsch and K. Yamamoto, *Flavour symmetries in the SMEFT*, *JHEP* **08** (2020) 166, [[2005.05366](#)].
- [49] A. Greljo, A. Palavrić and A. E. Thomsen, *Adding Flavor to the SMEFT*, *JHEP* **10** (2022) 010, [[2203.09561](#)].
- [50] F. Ferreira, B. Fuks, V. Sanz and D. Sengupta, *Probing CP-violating Higgs and gauge-boson couplings in the Standard Model effective field theory*, *Eur. Phys. J. C* **77** (2017) 675, [[1612.01808](#)].
- [51] J. Brehmer, F. Kling, T. Plehn and T. M. P. Tait, *Better Higgs-CP Tests Through Information Geometry*, *Phys. Rev. D* **97** (2018) 095017, [[1712.02350](#)].
- [52] F. U. Bernlochner, C. Englert, C. Hays, K. Lohwasser, H. Mildner, A. Pilkington et al., *Angles on CP-violation in Higgs boson interactions*, *Phys. Lett. B* **790** (2019) 372–379, [[1808.06577](#)].
- [53] C. Englert, P. Galler, A. Pilkington and M. Spannowsky, *Approaching robust EFT limits for CP-violation in the Higgs sector*, *Phys. Rev. D* **99** (2019) 095007, [[1901.05982](#)].

- [54] V. Cirigliano, A. Crivellin, W. Dekens, J. de Vries, M. Hoferichter and E. Mereghetti, *CP Violation in Higgs-Gauge Interactions: From Tabletop Experiments to the LHC*, *Phys. Rev. Lett.* **123** (2019) 051801, [[1903.03625](#)].
- [55] A. Biekötter, R. Gomez-Ambrosio, P. Gregg, F. Krauss and M. Schönherr, *Constraining SMEFT operators with associated  $h\gamma$  production in weak boson fusion*, *Phys. Lett. B* **814** (2021) 136079, [[2003.06379](#)].
- [56] A. Biekötter, P. Gregg, F. Krauss and M. Schönherr, *Constraining CP violating operators in charged and neutral triple gauge couplings*, *Phys. Lett. B* **817** (2021) 136311, [[2102.01115](#)].
- [57] S. D. Bakshi, J. Chakraborty, C. Englert, M. Spannowsky and P. Stylianou, *Landscaping CP-violating BSM scenarios*, *Nucl. Phys. B* **975** (2022) 115676, [[2103.15861](#)].
- [58] C. Degrande and J. Touch  que, *A reduced basis for CP violation in SMEFT at colliders and its application to diboson production*, *JHEP* **04** (2022) 032, [[2110.02993](#)].
- [59] A. Bhardwaj, C. Englert, R. Hankache and A. D. Pilkington, *Machine-enhanced CP-asymmetries in the Higgs sector*, *Phys. Lett. B* **832** (2022) 137246, [[2112.05052](#)].
- [60] N. C. Hall, I. Criddle, A. Crossland, C. Englert, P. Forbes, R. Hankache et al., *Machine-enhanced CP-asymmetries in the electroweak sector*, *Phys. Rev. D* **107** (2023) 016008, [[2209.05143](#)].
- [61] M. O. A. Thomas and E. Vryonidou, *CP violation in loop-induced diboson production*, [2411.00959](#).
- [62] M. Gonz  lez-Alonso and J. Martin Camalich, *Global Effective-Field-Theory analysis of New-Physics effects in (semi)leptonic kaon decays*, *JHEP* **12** (2016) 052, [[1605.07114](#)].
- [63] A. Falkowski, M. Gonz  lez-Alonso and O. Naviliat-Cuncic, *Comprehensive analysis of beta decays within and beyond the Standard Model*, *JHEP* **04** (2021) 126, [[2010.13797](#)].
- [64] V. Cirigliano, W. Dekens, J. de Vries, E. Mereghetti and T. Tong, *Beta-decay implications for the W-boson mass anomaly*, *Phys. Rev. D* **106** (2022) 075001, [[2204.08440](#)].
- [65] M. Thomas Arun, K. Deka and T. Srivastava, *Constraining SMEFT BSM scenarios with EWPO and  $\Delta_{CKM}$* , [2301.09273](#).
- [66] V. Cirigliano, W. Dekens, J. de Vries, E. Mereghetti and T. Tong, *Anomalies in global SMEFT analyses. A case study of first-row CKM unitarity*, *JHEP* **03** (2024) 033, [[2311.00021](#)].
- [67] ATLAS collaboration, M. Aaboud et al., *Measurement of  $W^\pm Z$  production cross sections and gauge boson polarisation in pp collisions at  $\sqrt{s} = 13$  TeV with the ATLAS detector*, *Eur. Phys. J. C* **79** (2019) 535, [[1902.05759](#)].
- [68] ATLAS collaboration, M. Aaboud et al., *Measurement of fiducial and differential  $W^+W^-$  production cross-sections at  $\sqrt{s} = 13$  TeV with the ATLAS detector*, *Eur. Phys. J. C* **79** (2019) 884, [[1905.04242](#)].
- [69] A. Biek  tter, B. D. Pecjak, D. J. Scott and T. Smith, *Electroweak input schemes and universal corrections in SMEFT*, *JHEP* **07** (2023) 115, [[2305.03763](#)].
- [70] D. M. Straub, *flavio: a Python package for flavour and precision phenomenology in the Standard Model and beyond*, [1810.08132](#).
- [71] A. Falkowski and K. Mimouni, *Model independent constraints on four-lepton operators*, *JHEP* **02** (2016) 086, [[1511.07434](#)].

- [72] L. Allwicher, D. A. Faroughy, F. Jaffredo, O. Sumensari and F. Wilsch, *HighPT: A tool for high- $p_T$  Drell-Yan tails beyond the standard model*, *Comput. Phys. Commun.* **289** (2023) 108749, [[2207.10756](#)].
- [73] I. Brivio, *SMEFTsim 3.0 — a practical guide*, *JHEP* **04** (2021) 073, [[2012.11343](#)].
- [74] C. Degrande, G. Durieux, F. Maltoni, K. Mimasu, E. Vryonidou and C. Zhang, *Automated one-loop computations in the standard model effective field theory*, *Phys. Rev. D* **103** (2021) 096024, [[2008.11743](#)].
- [75] A. Celis, J. Fuentes-Martin, A. Vicente and J. Virto, *DsixTools: The Standard Model Effective Field Theory Toolkit*, *Eur. Phys. J. C* **77** (2017) 405, [[1704.04504](#)].
- [76] J. Fuentes-Martin, P. Ruiz-Femenia, A. Vicente and J. Virto, *DsixTools 2.0: The Effective Field Theory Toolkit*, *Eur. Phys. J. C* **81** (2021) 167, [[2010.16341](#)].
- [77] E. E. Jenkins, A. V. Manohar and P. Stoffer, *Low-Energy Effective Field Theory below the Electroweak Scale: Operators and Matching*, *JHEP* **03** (2018) 016, [[1709.04486](#)].
- [78] E. E. Jenkins, A. V. Manohar and P. Stoffer, *Low-Energy Effective Field Theory below the Electroweak Scale: Anomalous Dimensions*, *JHEP* **01** (2018) 084, [[1711.05270](#)].
- [79] W. Dekens and P. Stoffer, *Low-energy effective field theory below the electroweak scale: matching at one loop*, *JHEP* **10** (2019) 197, [[1908.05295](#)].
- [80] K. Asteriadis, S. Dawson, P. P. Giardino and R. Szafron, *The  $e^+e^- \rightarrow ZH$  Process in the SMEFT Beyond Leading Order*, [2409.11466](#).
- [81] CMS collaboration, A. M. Sirunyan et al., *Measurement of double-differential cross sections for top quark pair production in  $pp$  collisions at  $\sqrt{s} = 8$  TeV and impact on parton distribution functions*, *Eur. Phys. J. C* **77** (2017) 459, [[1703.01630](#)].
- [82] CMS collaboration, S. Chatrchyan et al., *Measurement of the  $t\bar{t}$  production cross section in the dilepton channel in  $pp$  collisions at  $\sqrt{s} = 8$  TeV*, *JHEP* **02** (2014) 024, [[1312.7582](#)].
- [83] S. Dawson and P. P. Giardino, *Electroweak and QCD corrections to  $Z$  and  $W$  pole observables in the standard model EFT*, *Phys. Rev. D* **101** (2020) 013001, [[1909.02000](#)].
- [84] S. Dawson and P. P. Giardino, *Flavorful electroweak precision observables in the Standard Model effective field theory*, *Phys. Rev. D* **105** (2022) 073006, [[2201.09887](#)].
- [85] L. Alasfar, J. de Blas and R. Gröber, *Higgs probes of top quark contact interactions and their interplay with the Higgs self-coupling*, *JHEP* **05** (2022) 111, [[2202.02333](#)].
- [86] N. P. Hartland, F. Maltoni, E. R. Nocera, J. Rojo, E. Slade, E. Vryonidou et al., *A Monte Carlo global analysis of the Standard Model Effective Field Theory: the top quark sector*, *JHEP* **04** (2019) 100, [[1901.05965](#)].
- [87] Z. Kassabov, M. Madigan, L. Mantani, J. Moore, M. Morales Alvarado, J. Rojo et al., *The top quark legacy of the LHC Run II for PDF and SMEFT analyses*, *JHEP* **05** (2023) 205, [[2303.06159](#)].
- [88] R. Alonso, K. Kanshin and S. Saa, *Renormalization group evolution of Higgs effective field theory*, *Phys. Rev. D* **97** (2018) 035010, [[1710.06848](#)].
- [89] Z. Bern, J. Parra-Martinez and E. Sawyer, *Structure of two-loop SMEFT anomalous dimensions via on-shell methods*, *JHEP* **10** (2020) 211, [[2005.12917](#)].
- [90] Q. Jin, K. Ren and G. Yang, *Two-Loop anomalous dimensions of QCD operators up to dimension-sixteen and Higgs EFT amplitudes*, *JHEP* **04** (2021) 180, [[2011.02494](#)].

- [91] E. E. Jenkins, A. V. Manohar, L. Naterop and J. Pagès, *Two loop renormalization of scalar theories using a geometric approach*, *JHEP* **02** (2024) 131, [[2310.19883](#)].
- [92] J. Fuentes-Martín, A. Palavrić and A. E. Thomsen, *Functional matching and renormalization group equations at two-loop order*, *Phys. Lett. B* **851** (2024) 138557, [[2311.13630](#)].
- [93] A. Ibarra, N. Leister and D. Zhang, *Complete Two-loop Renormalization Group Equation of the Weinberg Operator*, [2411.08011](#).
- [94] ATLAS collaboration, M. Aaboud et al., *Search for low-mass resonances decaying into two jets and produced in association with a photon using pp collisions at  $\sqrt{s} = 13$  TeV with the ATLAS detector*, *Phys. Lett. B* **795** (2019) 56–75, [[1901.10917](#)].
- [95] ATLAS, CMS collaboration, G. Aad et al., *Measurements of the Higgs boson production and decay rates and constraints on its couplings from a combined ATLAS and CMS analysis of the LHC pp collision data at  $\sqrt{s} = 7$  and 8 TeV*, *JHEP* **08** (2016) 045, [[1606.02266](#)].
- [96] ATLAS collaboration, G. Aad et al., *Measurements of the Higgs boson production and decay rates and coupling strengths using pp collision data at  $\sqrt{s} = 7$  and 8 TeV in the ATLAS experiment*, *Eur. Phys. J.* **C76** (2016) 6, [[1507.04548](#)].
- [97] ATLAS collaboration, G. Aad et al., *A search for the  $Z\gamma$  decay mode of the Higgs boson in pp collisions at  $\sqrt{s} = 13$  TeV with the ATLAS detector*, *Phys. Lett. B* **809** (2020) 135754, [[2005.05382](#)].
- [98] ATLAS collaboration, G. Aad et al., *A search for the dimuon decay of the Standard Model Higgs boson with the ATLAS detector*, *Phys. Lett. B* **812** (2021) 135980, [[2007.07830](#)].
- [99] ATLAS COLLABORATION collaboration, *Measurements of Higgs boson production cross-sections in the  $H \rightarrow \tau^+\tau^-$  decay channel in pp collisions at  $\sqrt{s} = 13$  TeV with the ATLAS detector*, tech. rep., CERN, Geneva, Aug, 2021.
- [100] ATLAS collaboration, G. Aad et al., *Measurements of Higgs bosons decaying to bottom quarks from vector boson fusion production with the ATLAS experiment at  $\sqrt{s} = 13$  TeV*, *Eur. Phys. J. C* **81** (2021) 537, [[2011.08280](#)].
- [101] ATLAS collaboration, *Measurement of the Higgs boson decaying to b-quarks produced in association with a top-quark pair in pp collisions at  $\sqrt{s} = 13$  TeV with the ATLAS detector*, *ATLAS-CONF-2020-058* (11, 2020) .
- [102] ATLAS collaboration, *Interpretations of the combined measurement of Higgs boson production and decay*, *ATLAS-CONF-2020-053* (10, 2020) .
- [103] ATLAS collaboration, *Measurements of gluon fusion and vector-boson-fusion production of the Higgs boson in  $H \rightarrow WW^* \rightarrow e\nu\mu\nu$  decays using pp collisions at  $\sqrt{s} = 13$  TeV with the ATLAS detector*, *ATLAS-CONF-2021-014* (3, 2021) .
- [104] ATLAS collaboration, M. Aaboud et al., *Search for Higgs boson pair production in the  $\gamma\gamma b\bar{b}$  final state with 13 TeV pp collision data collected by the ATLAS experiment*, *JHEP* **11** (2018) 040, [[1807.04873](#)].
- [105] ATLAS collaboration, M. Aaboud et al., *Search for pair production of Higgs bosons in the  $b\bar{b}b\bar{b}$  final state using proton-proton collisions at  $\sqrt{s} = 13$  TeV with the ATLAS detector*, *JHEP* **01** (2019) 030, [[1804.06174](#)].
- [106] ATLAS collaboration, M. Aaboud et al., *Search for resonant and non-resonant Higgs boson*

- pair production in the  $b\bar{b}\tau^+\tau^-$  decay channel in  $pp$  collisions at  $\sqrt{s} = 13$  TeV with the ATLAS detector, *Phys. Rev. Lett.* **121** (2018) 191801, [1808.00336].
- [107] CMS collaboration, *Combined Higgs boson production and decay measurements with up to 137 fb<sup>-1</sup> of proton-proton collision data at  $\sqrt{s} = 13$  TeV*, CMS-PAS-HIG-19-005 (2020) .
- [108] CMS collaboration, A. M. Sirunyan et al., *Measurement of the inclusive and differential Higgs boson production cross sections in the leptonic WW decay mode at  $\sqrt{s} = 13$  TeV*, *JHEP* **03** (2021) 003, [2007.01984].
- [109] CMS collaboration, A. M. Sirunyan et al., *Evidence for Higgs boson decay to a pair of muons*, *JHEP* **01** (2021) 148, [2009.04363].
- [110] CMS collaboration, A. M. Sirunyan et al., *Measurement of the Higgs boson production rate in association with top quarks in final states with electrons, muons, and hadronically decaying tau leptons at  $\sqrt{s} = 13$  TeV*, *Eur. Phys. J. C* **81** (2021) 378, [2011.03652].
- [111] CMS collaboration, *Measurement of Higgs boson production in association with a W or Z boson in the  $H \rightarrow WW$  decay channel*, CMS-PAS-HIG-19-017 (2021) .
- [112] CMS collaboration, *Measurement of Higgs boson production in the decay channel with a pair of  $\tau$  leptons*, CMS-PAS-HIG-19-010 (2020) .
- [113] CMS collaboration, A. M. Sirunyan et al., *Measurements of Higgs boson production cross sections and couplings in the diphoton decay channel at  $\sqrt{s} = 13$  TeV*, *JHEP* **07** (2021) 027, [2103.06956].
- [114] CMS collaboration, A. M. Sirunyan et al., *Measurements of production cross sections of the Higgs boson in the four-lepton final state in proton-proton collisions at  $\sqrt{s} = 13$  TeV*, *Eur. Phys. J. C* **81** (2021) 488, [2103.04956].
- [115] CMS collaboration, A. M. Sirunyan et al., *Search for nonresonant Higgs boson pair production in final states with two bottom quarks and two photons in proton-proton collisions at  $\sqrt{s} = 13$  TeV*, *JHEP* **03** (2021) 257, [2011.12373].
- [116] CMS collaboration, *Search for Higgs boson pair production in the four b quark final state*, CMS-PAS-HIG-20-005 (2021) .
- [117] CMS collaboration, A. M. Sirunyan et al., *Search for Higgs boson pair production in events with two bottom quarks and two tau leptons in proton-proton collisions at  $\sqrt{s} = 13$  TeV*, *Phys. Lett. B* **778** (2018) 101–127, [1707.02909].
- [118] ATLAS collaboration, G. Aad et al., *Differential cross-section measurements for the electroweak production of dijets in association with a Z boson in proton-proton collisions at ATLAS*, *Eur. Phys. J. C* **81** (2021) 163, [2006.15458].
- [119] CDF, D0 collaboration, T. A. Aaltonen et al., *Combined Forward-Backward Asymmetry Measurements in Top-Antitop Quark Production at the Tevatron*, *Phys. Rev. Lett.* **120** (2018) 042001, [1709.04894].
- [120] ATLAS, CMS collaboration, M. Aaboud et al., *Combination of inclusive and differential  $t\bar{t}$  charge asymmetry measurements using ATLAS and CMS data at  $\sqrt{s} = 7$  and 8 TeV*, *JHEP* **04** (2018) 033, [1709.05327].
- [121] CMS, ATLAS collaboration, G. Aad et al., *Combination of the W boson polarization measurements in top quark decays using ATLAS and CMS data at  $\sqrt{s} = 8$  TeV*, *JHEP* **08** (2020) 051, [2005.03799].



- [122] ATLAS collaboration, G. Aad et al., *Measurements of the charge asymmetry in top-quark pair production in the dilepton final state at  $\sqrt{s} = 8$  TeV with the ATLAS detector*, *Phys. Rev. D* **94** (2016) 032006, [[1604.05538](#)].
- [123] ATLAS collaboration, G. Aad et al., *Measurement of the  $t\bar{t}W$  and  $t\bar{t}Z$  production cross sections in  $pp$  collisions at  $\sqrt{s} = 8$  TeV with the ATLAS detector*, *JHEP* **11** (2015) 172, [[1509.05276](#)].
- [124] ATLAS collaboration, M. Aaboud et al., *Fiducial, total and differential cross-section measurements of  $t$ -channel single top-quark production in  $pp$  collisions at 8 TeV using data collected by the ATLAS detector*, *Eur. Phys. J. C* **77** (2017) 531, [[1702.02859](#)].
- [125] ATLAS collaboration, G. Aad et al., *Measurement of single top-quark production in association with a  $W$  boson in the single-lepton channel at  $\sqrt{s} = 8$  TeV with the ATLAS detector*, *Eur. Phys. J. C* **81** (2021) 720, [[2007.01554](#)].
- [126] ATLAS collaboration, G. Aad et al., *Measurement of the production cross-section of a single top quark in association with a  $W$  boson at 8 TeV with the ATLAS experiment*, *JHEP* **01** (2016) 064, [[1510.03752](#)].
- [127] ATLAS collaboration, G. Aad et al., *Evidence for single top-quark production in the  $s$ -channel in proton-proton collisions at  $\sqrt{s} = 8$  TeV with the ATLAS detector using the Matrix Element Method*, *Phys. Lett. B* **756** (2016) 228–246, [[1511.05980](#)].
- [128] ATLAS collaboration, M. Aaboud et al., *Measurement of top quark pair differential cross-sections in the dilepton channel in  $pp$  collisions at  $\sqrt{s} = 7$  and 8 TeV with ATLAS*, *Phys. Rev. D* **94** (2016) 092003, [[1607.07281](#)].
- [129] ATLAS collaboration, G. Aad et al., *Measurements of top-quark pair differential cross-sections in the lepton+jets channel in  $pp$  collisions at  $\sqrt{s} = 8$  TeV using the ATLAS detector*, *Eur. Phys. J. C* **76** (2016) 538, [[1511.04716](#)].
- [130] CMS collaboration, V. Khachatryan et al., *Observation of top quark pairs produced in association with a vector boson in  $pp$  collisions at  $\sqrt{s} = 8$  TeV*, *JHEP* **01** (2016) 096, [[1510.01131](#)].
- [131] CMS collaboration, V. Khachatryan et al., *Measurements of  $t\bar{t}$  charge asymmetry using dilepton final states in  $pp$  collisions at  $\sqrt{s} = 8$  TeV*, *Phys. Lett. B* **760** (2016) 365–386, [[1603.06221](#)].
- [132] CMS collaboration, A. M. Sirunyan et al., *Measurement of the semileptonic  $t\bar{t} + \gamma$  production cross section in  $pp$  collisions at  $\sqrt{s} = 8$  TeV*, *JHEP* **10** (2017) 006, [[1706.08128](#)].
- [133] CMS collaboration, V. Khachatryan et al., *Search for  $s$  channel single top quark production in  $pp$  collisions at  $\sqrt{s} = 7$  and 8 TeV*, *JHEP* **09** (2016) 027, [[1603.02555](#)].
- [134] CMS collaboration, *Single top  $t$ -channel differential cross section at 8 TeV*, *CMS-PAS-TOP-14-004* (2014) .
- [135] CMS collaboration, V. Khachatryan et al., *Measurement of the  $t$ -channel single-top-quark production cross section and of the  $|V_{tb}|$  CKM matrix element in  $pp$  collisions at  $\sqrt{s} = 8$  TeV*, *JHEP* **06** (2014) 090, [[1403.7366](#)].
- [136] CMS collaboration, S. Chatrchyan et al., *Observation of the associated production of a single top quark and a  $W$  boson in  $pp$  collisions at  $\sqrt{s} = 8$  TeV*, *Phys. Rev. Lett.* **112** (2014) 231802, [[1401.2942](#)].

- [137] CMS collaboration, V. Khachatryan et al., *Measurement of the differential cross section for top quark pair production in pp collisions at  $\sqrt{s} = 8$  TeV*, *Eur. Phys. J. C* **75** (2015) 542, [[1505.04480](#)].
- [138] CMS collaboration, V. Khachatryan et al., *Measurements of the  $t\bar{t}$  production cross section in lepton+jets final states in pp collisions at 8 TeV and ratio of 8 to 7 TeV cross sections*, *Eur. Phys. J. C* **77** (2017) 15, [[1602.09024](#)].
- [139] ATLAS collaboration, M. Aaboud et al., *Measurement of the cross-section for producing a W boson in association with a single top quark in pp collisions at  $\sqrt{s} = 13$  TeV with ATLAS*, *JHEP* **01** (2018) 063, [[1612.07231](#)].
- [140] ATLAS collaboration, M. Aaboud et al., *Measurement of the production cross-section of a single top quark in association with a Z boson in proton-proton collisions at 13 TeV with the ATLAS detector*, *Phys. Lett. B* **780** (2018) 557–577, [[1710.03659](#)].
- [141] ATLAS collaboration, M. Aaboud et al., *Measurement of the inclusive cross-sections of single top-quark and top-antiquark t-channel production in pp collisions at  $\sqrt{s} = 13$  TeV with the ATLAS detector*, *JHEP* **04** (2017) 086, [[1609.03920](#)].
- [142] ATLAS collaboration, *Inclusive and differential measurement of the charge asymmetry in  $t\bar{t}$  events at 13 TeV with the ATLAS detector*, ATLAS-CONF-2019-026 (7, 2019) .
- [143] ATLAS collaboration, M. Aaboud et al., *Measurement of the  $t\bar{t}Z$  and  $t\bar{t}W$  cross sections in proton-proton collisions at  $\sqrt{s} = 13$  TeV with the ATLAS detector*, *Phys. Rev. D* **99** (2019) 072009, [[1901.03584](#)].
- [144] ATLAS collaboration, G. Aad et al., *Measurements of inclusive and differential cross-sections of combined  $t\bar{t}\gamma$  and  $tW\gamma$  production in the  $e\mu$  channel at 13 TeV with the ATLAS detector*, *JHEP* **09** (2020) 049, [[2007.06946](#)].
- [145] CMS collaboration, A. M. Sirunyan et al., *Measurement of the production cross section for single top quarks in association with W bosons in proton-proton collisions at  $\sqrt{s} = 13$  TeV*, *JHEP* **10** (2018) 117, [[1805.07399](#)].
- [146] CMS collaboration, A. M. Sirunyan et al., *Observation of Single Top Quark Production in Association with a Z Boson in Proton-Proton Collisions at  $\sqrt{s} = 13$  TeV*, *Phys. Rev. Lett.* **122** (2019) 132003, [[1812.05900](#)].
- [147] CMS collaboration, A. M. Sirunyan et al., *Measurement of differential cross sections and charge ratios for t-channel single top quark production in proton-proton collisions at  $\sqrt{s} = 13$  TeV*, *Eur. Phys. J. C* **80** (2020) 370, [[1907.08330](#)].
- [148] CMS collaboration, A. M. Sirunyan et al., *Measurement of the  $t\bar{t}$  production cross section, the top quark mass, and the strong coupling constant using dilepton events in pp collisions at  $\sqrt{s} = 13$  TeV*, *Eur. Phys. J. C* **79** (2019) 368, [[1812.10505](#)].
- [149] CMS collaboration, *Measurement of differential  $t\bar{t}$  production cross sections in the full kinematic range using lepton+jets events from pp collisions at  $\sqrt{s} = 13$  TeV*, CMS-PAS-TOP-20-001 (2021) .
- [150] CMS collaboration, A. M. Sirunyan et al., *Measurement of the cross section for top quark pair production in association with a W or Z boson in proton-proton collisions at  $\sqrt{s} = 13$  TeV*, *JHEP* **08** (2018) 011, [[1711.02547](#)].
- [151] CMS collaboration, A. M. Sirunyan et al., *Measurement of top quark pair production in*

- association with a  $Z$  boson in proton-proton collisions at  $\sqrt{s} = 13$  TeV, *JHEP* **03** (2020) 056, [[1907.11270](#)].
- [152] CMS collaboration, A. M. Sirunyan et al., *Search for resonant and nonresonant new phenomena in high-mass dilepton final states at  $\sqrt{s} = 13$  TeV*, *JHEP* **07** (2021) 208, [[2103.02708](#)].
- [153] ATLAS collaboration, G. Aad et al., *Search for heavy Higgs bosons decaying into two tau leptons with the ATLAS detector using pp collisions at  $\sqrt{s} = 13$  TeV*, *Phys. Rev. Lett.* **125** (2020) 051801, [[2002.12223](#)].
- [154] ALEPH, DELPHI, L3, OPAL, SLD, LEP ELECTROWEAK WORKING GROUP, SLD ELECTROWEAK GROUP, SLD HEAVY FLAVOUR GROUP collaboration, S. Schael et al., *Precision electroweak measurements on the  $Z$  resonance*, *Phys. Rept.* **427** (2006) 257–454, [[hep-ex/0509008](#)].
- [155] PARTICLE DATA GROUP collaboration, C. Patrignani et al., *Review of Particle Physics*, *Chin. Phys. C* **40** (2016) 100001.
- [156] QWEAK collaboration, D. Androic et al., *First Determination of the Weak Charge of the Proton*, *Phys. Rev. Lett.* **111** (2013) 141803, [[1307.5275](#)].
- [157] PVDIS collaboration, D. Wang et al., *Measurement of parity violation in electron–quark scattering*, *Nature* **506** (2014) 67–70.
- [158] E. J. Beise, M. L. Pitt and D. T. Spayde, *The SAMPLE experiment and weak nucleon structure*, *Prog. Part. Nucl. Phys.* **54** (2005) 289–350, [[nucl-ex/0412054](#)].
- [159] VENUS collaboration, H. Hanai et al., *Measurement of tau polarization in  $e^+e^-$  annihilation at  $s^{*(1/2)} = 58$ -GeV*, *Phys. Lett. B* **403** (1997) 155–162, [[hep-ex/9703003](#)].
- [160] ALEPH, DELPHI, L3, OPAL, LEP ELECTROWEAK collaboration, S. Schael et al., *Electroweak Measurements in Electron-Positron Collisions at  $W$ -Boson-Pair Energies at LEP*, *Phys. Rept.* **532** (2013) 119–244, [[1302.3415](#)].
- [161] LEP, ALEPH, DELPHI, L3, OPAL, LEP ELECTROWEAK WORKING GROUP, SLD ELECTROWEAK GROUP, SLD HEAVY FLAVOR GROUP collaboration, t. S. Electroweak, *A Combination of preliminary electroweak measurements and constraints on the standard model*, [[hep-ex/0312023](#)].
- [162] LHCb collaboration, R. Aaij et al., *Differential branching fractions and isospin asymmetries of  $B \rightarrow K^{(*)}\mu^+\mu^-$  decays*, *JHEP* **06** (2014) 133, [[1403.8044](#)].
- [163] CMS collaboration, V. Khachatryan et al., *Angular analysis of the decay  $B^0 \rightarrow K^{*0}\mu^+\mu^-$  from pp collisions at  $\sqrt{s} = 8$  TeV*, *Phys. Lett. B* **753** (2016) 424–448, [[1507.08126](#)].
- [164] LHCb collaboration, R. Aaij et al., *Differential branching fraction and angular analysis of  $\Lambda_b^0 \rightarrow \Lambda\mu^+\mu^-$  decays*, *JHEP* **06** (2015) 115, [[1503.07138](#)].
- [165] BABAR collaboration, J. P. Lees et al., *Measurement of the  $B \rightarrow X_s l^+ l^-$  branching fraction and search for direct CP violation from a sum of exclusive final states*, *Phys. Rev. Lett.* **112** (2014) 211802, [[1312.5364](#)].
- [166] A. Greljo, J. Salko, A. Smolkovič and P. Stangl, *Rare  $b$  decays meet high-mass Drell-Yan*, *JHEP* **05** (2023) 087, [[2212.10497](#)].
- [167] M. Misiak and M. Steinhauser, *Weak radiative decays of the  $B$  meson and bounds on  $M_{H^\pm}$  in the Two-Higgs-Doublet Model*, *Eur. Phys. J. C* **77** (2017) 201, [[1702.04571](#)].

- [168] HFLAV collaboration, Y. Amhis et al., *Averages of b-hadron, c-hadron, and  $\tau$ -lepton properties as of summer 2014*, [1412.7515](#).
- [169] BABAR collaboration, J. P. Lees et al., *Search for  $B \rightarrow K^{(*)} \nu \bar{\nu}$  and invisible quarkonium decays*, *Phys. Rev. D* **87** (2013) 112005, [[1303.7465](#)].
- [170] BELLE collaboration, D. Dutta et al., *Search for  $B_s^0 \rightarrow \gamma\gamma$  and a measurement of the branching fraction for  $B_s^0 \rightarrow \phi\gamma$* , *Phys. Rev. D* **91** (2015) 011101, [[1411.7771](#)].
- [171] PARTICLE DATA GROUP collaboration, R. L. Workman et al., *Review of Particle Physics*, *PTEP* **2022** (2022) 083C01.
- [172] LHCb collaboration, .  $\rightarrow K + + -$  et al., *Measurement of lepton universality parameters in  $B^+ \rightarrow K^+ \ell^+ \ell^-$  and  $B^0 \rightarrow K^{*0} \ell^+ \ell^-$  decays*, *Phys. Rev. D* **108** (2023) 032002, [[2212.09153](#)].
- [173] HFLAV collaboration, Y. Amhis et al., *Averages of b-hadron, c-hadron, and  $\tau$ -lepton properties as of summer 2016*, *Eur. Phys. J. C* **77** (2017) 895, [[1612.07233](#)].
- [174] PARTICLE DATA GROUP collaboration, M. Tanabashi et al., *Review of Particle Physics*, *Phys. Rev. D* **98** (2018) 030001.
- [175] LHCb collaboration, R. Aaij et al., *Measurement of CP-Averaged Observables in the  $B^0 \rightarrow K^{*0} \mu^+ \mu^-$  Decay*, *Phys. Rev. Lett.* **125** (2020) 011802, [[2003.04831](#)].